Spectra of water dimer from a new ab initio potential with flexible monomers

Claude Leforestier, Krzysztof Szalewicz, and Ad van der Avoird

Citation: J. Chem. Phys. **137**, 014305 (2012); doi: 10.1063/1.4722338
View online: http://dx.doi.org/10.1063/1.4722338
View Table of Contents: http://jcp.aip.org/resource/1/JCPSA6/v137/i1
Published by the American Institute of Physics.

Spectra of water dimer from a new *ab initio* potential with flexible monomers

Claude Leforestier,[1,a)] Krzysztof Szalewicz,[2,b)] and Ad van der Avoird[3,c)]
[1]*Institut Charles Gerhardt (CTMM)-UMR 5253, CC 1501, Université Montpellier II-CNRS, 34095 Montpellier Cedex 05, France*
[2]*Department of Physics and Astronomy, University of Delaware, Newark, Delaware 19716, USA*
[3]*Theoretical Chemistry, Institute for Molecules and Materials, Radboud University Nijmegen, Heyendaalseweg 135, 6525 AJ Nijmegen, The Netherlands*

(Received 29 March 2012; accepted 11 May 2012; published online 5 July 2012)

We report the definition and testing of a new *ab initio* 12-dimensional potential for the water dimer with flexible monomers. Using our recent accurate CCpol-8s rigid water pair potential [W. Cencek, K. Szalewicz, C. Leforestier, R. van Harrevelt, and A. van der Avoird, Phys. Chem. Chem. Phys. **10**, 4716 (2008)] as a reference for the undistorted monomers' geometries, a distortion correction has been added, which was taken from a former flexible-monomer *ab initio* potential. This correction allows us to retrieve the correct binding energy $D_e = 21.0\ \text{kJ mol}^{-1}$, and leads to an equilibrium geometry in close agreement with the one obtained from benchmark calculations. The kinetic energy operator describing the flexible-monomer water dimer has been expressed in terms of Radau coordinates for each monomer and a recent general cluster polyspherical formulation describing their relative motions. Within this formulation, an adiabatic scheme has been invoked in order to decouple fast (intramolecular) modes and slow (intermolecular) ones. Different levels of approximation were tested, which differ in the way in which the residual potential coupling between the intramolecular modes located on different monomers and the dependence of the monomer rotational constants on the dimer geometry are handled. Accurate calculations of the vibration-rotation-tunneling levels of $(H_2O)_2$ and $(D_2O)_2$ were performed, which show the best agreement with experiments achieved so far for any water potential. Intramolecular excitations of the two monomers were calculated within two limiting cases, to account for the lack of non-adiabatic coupling between intramolecular modes due to the intermolecular motion. In the first model, the excitation was assumed to stay either on the donor or the acceptor molecule, and to hop between the two moieties upon donor-acceptor interchange. In the second model, the excitation remains on the same molecule whatever is the dimer geometry. Marginal frequency differences, less than $2\ \text{cm}^{-1}$, were obtained for all modes, and the resulting infrared shifts are in good agreement with experiments. © *2012 American Institute of Physics*. [http://dx.doi.org/10.1063/1.4722338]

I. INTRODUCTION

Water dimer is the subject of continuous theoretical and experimental interest.[1] This is due to both the importance of the isolated dimer, in particular for atmospheric science,[2,3] and to the fact that the dimer interactions constitute the leading and most important term in a many-body expansion for water clusters and condensed phases of water.[1,4] The main source of experimental information on water dimer comes from spectral measurements.[5–9] The quest to reproduce the intermolecular rovibrational transitions began in the late 1990s when six-dimensional (6D) "exact" quantum nuclear dynamics calculations became possible.[10–13] In such calculations, the monomers are kept rigid, preferably at their average ground rovibrational state configuration.[14,15] The vibrations and hindered rotations of the monomers in the water dimer have large amplitudes and are highly anharmonic, so that nearly exact quantum dynamics is absolutely necessary to quantitatively describe the transitions between the intermolecular rovibrational levels. In addition, these levels are split by quantum tunneling and the harmonic approximation fails to give even a qualitatively correct spectrum. The standard methods improving upon this approximation predict transitions with large errors. It has been found in the early calculations that even if fully anharmonic quantum dynamics is used, none of the existing water dimer potentials gives even a qualitatively correct description of the measured spectrum. However, it was possible to fit a potential to spectral data and to model the spectrum well.[11] The first *ab initio* potential to achieve a fairly accurate description of the spectrum was the SAPT-5s potential developed in Refs. 13, 16, and 17. With two recent water pair potentials,[18,19] it became possible to reach nearly perfect agreement of the intermolecular mode frequencies and tunneling splittings with the measured high-resolution spectra.

The next challenge in investigations of water dimer was to go beyond the rigid-monomer approximation. This extension allows in particular the computation of the shifts of intra-monomer fundamental infrared (IR) vibrational

a)Electronic mail: claude.leforestier@univ-montp2.fr.
b)Electronic mail: szalewic@udel.edu.
c)Electronic mail: A.vanderAvoird@theochem.ru.nl.

transitions. These shifts are subjects of numerous measurements for hydrogen-bonded dimers and constitute a signature of the presence of hydrogen bonds. Although some of the IR shifts in the water dimer have been measured more than two decades ago,[5,20,21] new experimental data are still becoming available[9] and part of the existing data have been reassigned. The agreement between the previously calculated frequency shifts and the experimental data is still not as good as it is for the intermolecular modes. Whereas "exact" 12-dimensional (12D) calculations are still not possible, a [6+6]D adiabatic decoupling method developed by one of the present authors and co-workers[22] is sufficiently accurate for the water dimer. This method was initially used to fit an empirical potential to the spectra.[22] The only flexible-monomer water-dimer potentials available until the early 2000s were empirical ones fitted to bulk water properties with the inter-intramolecular couplings achieved only by the "atom-following" approach in atom-atom potential functional forms, i.e., by allowing the monomers to deform without changing the interatomic parameters. Such an approach gives only a qualitative description of the couplings.[23,24] The first fully *ab initio* 12-dimensional water pair potentials were developed in Refs. 25 and 26. The potential in Ref. 25 was based on interaction energies calculated on a grid of almost a quarter million flexible-monomer geometries using symmetry-adapted perturbation theory (SAPT).[27,28] The level of SAPT and the basis set was the same as used to develop the SAPT-5s potential[13,16,17] and the two developed 12-dimensional potentials were called SAPT-5s′*f* and SAPT-5s′*f*IR, where "*f*" stands for "flexible monomer" and the prime indicates a modification of the rigid-monomer functional form relative to the original SAPT-5s potential. The SAPT-5s′*f*IR potential differed from SAPT-5s′*f* by using in the fitting procedure the Hessian of the potential at the dimer equilibrium. This Hessian was computed from *ab initio* interaction energies by numerical differentiation. The SAPT-5s′*f*IR performed much better in spectral predictions than SAPT-5s′*f*, and only this potential will be considered here. For intermonomer transitions, the predictions from flexible-monomer calculations[25] were very similar to those from rigid-monomer ones, which shows that the effects of monomer flexibility on these transitions are small. The predictions for the intra-monomer IR shifts were in good agreement with experiment, with a root-mean-square deviation (rmsd) of only 8 cm^{-1}. This result can be compared to the best *ab initio* harmonic calculations of the shifts (from numerical Hessians) which gave errors of 26 cm^{-1} (Ref. 29) or 12 cm^{-1} (Ref. 30). One should mention here that simple harmonic calculations predict IR frequency shifts reasonably well, in contrast to predictions of the intermonomer transition frequencies. Incidentally, the harmonic shifts computed directly from numerical SAPT Hessians and the harmonic SAPT-5s′*f*IR shifts gave the smallest rmsd of 6 cm^{-1}. The differences between harmonic and anharmonic SAPT-5s′*f*IR shifts ranged between −9 and 11 cm^{-1}, and provided the first estimate of the importance of anharmonic effects in calculations of IR shifts. However, part of this effect is due to the inadequacy of the potential fit, as the differences between SAPT-5s′*f*IR and SAPT harmonic frequencies ranged from −4 to 18 cm^{-1}. The flexible-monomer water dimer potential developed by Huang *et al.*[26] (we will denote this potential as HBB0) was based on 19 805 *ab initio* points computed at the coupled-cluster level with single, double, and noniterative triple excitations [CCSD(T)] in an augmented triple-zeta quality basis set. Due to the larger basis set than used in the development of SAPT-5s′*f*IR, the interaction energies of Huang *et al.* are more accurate, but the number of grid points is much smaller than in the case of SAPT-5s′*f*IR. An improved version of HBB0 (denoted as HBB), based on 30 000 grid points, was used in Ref. 19 in its rigid-monomer version to compute intermonomer spectral transitions. The agreement with experiment was very good, slightly better than that given earlier by the CCpol-5s potential of Refs. 31–33 but not as good as that given by the CCpol-8s potential.[18] The IR shifts predicted by the HBB potential, calculated in Ref. 34, were relatively poor, with a rmsd of 15 cm^{-1}.

In the present paper, we combine the currently most accurate rigid-monomer water dimer potential, CCpol-8s, with SAPT-5s′*f*IR. Such a combination is possible since SAPT-5s′*f*IR was constructed in such a way that if both monomers are in their average ground vibrational state geometries, SAPT-5s′*f*IR becomes identical with the SAPT-5s′ rigid-monomer potential. Thus, if one subtracts SAPT-5s′ and adds CCpol-8s, such a potential extends CCpol-8s to 12 dimensions by including monomer deformation effects at the level of SAPT-5s′*f*IR. The new potential has been used by us to compute the spectra of water dimer.

The outline of this paper is as follows. In Sec. II, we briefly recall our previous high accuracy rigid CCpol-8s and flexible-monomer SAPT-5s′*f*IR potentials which we combine here to define a new flexible-monomer potential. Section III introduces the adiabatic formulation which allows us to handle flexible monomers. Section IV presents the resulting microwave (MW) and far infrared spectra, as well as the infrared shifts, and comparison to experiments. Finally, some conclusions are drawn in Sec. V.

II. A FLEXIBLE CCPOL-8S POTENTIAL

Recently, Cencek *et al.*[18] proposed an accurate analytical representation of the water pair potential, denoted CCpol-8s. This rigid-monomer potential was obtained from a refitting of previous supermolecular calculations that used second-order perturbation theory with the Møller-Plesset decomposition of the Hamiltonian in combination with the CCSD(T) method.[31] The functional form of this potential is given by

$$V^{(2)} = \sum_{a\in A}^{\text{sites}} \sum_{b\in B}^{\text{sites}} u_{ab}(r_{ab}) + V_2^{\text{ind}}(A, B), \tag{1}$$

where

$$V_2^{\text{ind}}(A, B) = -\frac{1}{2}\left\{\boldsymbol{\mu}_A^{\text{ind}} \cdot \boldsymbol{F}^A + \boldsymbol{\mu}_B^{\text{ind}} \cdot \boldsymbol{F}^B\right\} \tag{2}$$

represents the induction term with the induced dipole moments $\boldsymbol{\mu}_A^{\text{ind}}$ and $\boldsymbol{\mu}_B^{\text{ind}}$ and electric fields $\boldsymbol{F}^A$ and $\boldsymbol{F}^B$ on the monomers. The fields are produced by only the static (permanent) fractional point charges. In contrast, the induced dipole moments are fully iterated, i.e., are proportional to the electric fields produced by both the static charges and the induced

dipole on the interacting partner. The site-site potentials u_{ab} depend only on the distances r_{ab} and have the following general form:

$$u_{ab}(r_{ab}) = f_1\left(\delta_{ab}^{(1)}, r_{ab}\right)\frac{q_a\, q_b}{r_{ab}} + e^{-\beta_{ab} r_{ab}} \sum_{m=0}^{3} c_{ab}^{(m)} r_{ab}^{m} + \sum_{n=6,8,10} f_n\left(\delta_{ab}^{(n)}, r_{ab}\right) C_{ab}^{(n)} r_{ab}^{-n}, \quad (3)$$

with $f_n(\delta, r)$ representing Tang-Toennies[35] damping functions. The improvement with respect to the CCpol-5s potential[31,32] came from using the same site-site form interaction potential but with eight symmetry-nonequivalent sites on each monomer, instead of five previously, and a better optimization of the locations of these sites. As a result, the root-mean-square error of the fit with respect to the *ab initio* data decreased from 0.089 to 0.010 kcal/mol for the data points with negative interaction energies. This new rigid-monomer potential, based on vibrationally averaged monomer geometries, produced a dimer vibration-rotation-tunneling (VRT) spectrum in substantially better agreement with high-resolution experimental data than the already quite accurate one predicted by CCpol-5s. Although CCpol-8s is close to the limit that might be expected for a rigid monomer potential, the lack of monomer flexibility precludes consideration of the IR frequency shifts of the monomer vibrations which constitute a signature of hydrogen bonding in the water dimer. Also other properties, such as the second virial coefficient,[3] are sensitive to flexibility as it changes the binding energy D_e.

Previously, we obtained a flexible-monomer water dimer potential from *ab initio* calculations performed with SAPT at about a quarter million grid points with non-rigid monomers.[25] A flexible-monomer 12-dimensional potential, denoted SAPT-5s′*f*IR, was fitted to these points by means of a similar site-site form as in Eqs. (1)–(3), but using only five nonequivalent sites on each monomer and a perturbative (noniterated) induction term

$$V_2^{\rm ind}(A, B) = -\frac{1}{2}\{\bar{\alpha}^A |\boldsymbol{F}^A|^2 + \bar{\alpha}^B |\boldsymbol{F}^B|^2\} f_6(\delta_d^{(6)}, R), \quad (4)$$

with $\bar{\alpha}^A$ and $\bar{\alpha}^B$ being the molecular polarizabilities and R the distance between polarization centers. This induction term contains a similar type of damping function as used in the other long range terms, while the CCpol-8s potential has an undamped but fully iterated induction term. To account for the energy variation upon distortion of the monomers, all the parameters $(q_a, q_b, \delta_{ab}^{(i)}, \beta_{ab}, c_{ab}^{(m)}, C_{ab}^{(i)})$ entering Eqs. (1), (3) and (4) were made dependent on the distortion $\mathbf{q}^X - \mathbf{q}_{\rm ref}$ of each monomer. The symbol $\mathbf{q}^X$ stands for the set of three internal coordinates of monomer $X(= A, B)$, and $\mathbf{q}_{\rm ref}$ refers to a reference geometry, for which we take the vibrationally averaged structure. The quality of this flexible-monomer potential surface can be checked, among other things, by comparing the characteristics of the global minimum with the benchmark calculations of Tschumper *et al.*[30] Table I shows (the dimer interatomic distances and angles are defined in Fig. 1) that intermonomer parameters are reproduced by SAPT-5s′*f*IR with a few-percent errors: the binding energy D_e with 5.2%, the equilibrium distance O_a–H_b with 3.0%, and the angle HO_aO_d with 1.7% error. It was demonstrated by Bukowski *et al.*[32] that deficiencies of SAPT-5s compared to CCpol-5s result mainly from the smaller basis set used to develop the former potential.

TABLE I. Binding energy D_e and fully optimized minimum geometry (see Fig. 1) as given by the benchmark calculations of Tschumper *et al.*,[30] the SAPT-5s′*f*IR and CCpol-8s*f* potentials. The subscripts *d* and *a* denote the donor and acceptor H_2O molecule, the subscripts *b* and *f* refer to the bound and free H atom of the donor, respectively.

	Ref. 30	SAPT-5s′*f*IR	CCpol-8s*f*
D_e	21.0	19.9	21.0 kJ/mol
O_d–H_f	0.958	0.956	0.957 Å
O_d–H_b	0.966	0.961	0.962 Å
O_a–H	0.960	0.958	0.959 Å
O_a–H_b	1.948	2.006	1.956 Å
$H_fO_dH_b$ angle	104.45	104.77	104.69°
HO_aH angle	104.58	104.99	104.68°
$O_dH_bO_a$ angle	172.92	171.64	171.74°
HO_aO_d angle	110.50	112.36	109.67°

In order to add flexibility to the recent very accurate CCpol-8s potential, we used the following simple prescription to define the pair potential $V^{(2)}_{\rm CCpol\text{-}8s\,f}$:

$$V^{(2)}_{\rm CCpol\text{-}8s\,f}(\mathbf{d}) = V^{(2)}_{\rm CCpol\text{-}8s}(\mathbf{u}) + V^{(2)}_{\rm SAPT\text{-}5s'\,f\,IR}(\mathbf{d}) - V^{(2)}_{\rm SAPT\text{-}5s'}(\mathbf{u}), \quad (5)$$

where **d** and **u** refer to geometries with distorted and the corresponding undistorted monomers, respectively. The latter implies that both monomers are at their reference geometry $\mathbf{q}_{\rm ref}$. Merging the two potentials as indicated above is actually possible because the $\mathbf{q}_{\rm ref}$ geometry defined in SAPT-5s′*f*IR corresponds to the same vibrationally averaged H_2O geometry as used for the rigid monomers in CCpol-8s. The definition given above relies on the assumption that the intrinsic errors of SAPT-5s′*f*IR, due to the lower accuracy level of the method, are similar for distorted and undistorted geometries. The difference $V_{\rm SAPT\text{-}5s'\,f\,IR}(\mathbf{d}) - V_{\rm SAPT\text{-}5s'}(\mathbf{u})$ thus represents the flexibility correction to be applied to the $V_{\rm CCpol\text{-}8s}(\mathbf{u})$ potential obtained for rigid monomers.

In the bound-state calculations, the 12D geometry of the system is described by two sets of coordinates: (i) the intermolecular coordinates, denoted by $\mathbf{Q} = (\mathcal{R}, \boldsymbol{\Omega}^A, \boldsymbol{\Omega}^B)$, which determine the center-of-mass separation $\mathcal{R}$ and the relative orientations of the two monomer-fixed frames, and (ii) the intramolecular ones $(\mathbf{q}^A, \mathbf{q}^B)$ that specify the geometry of

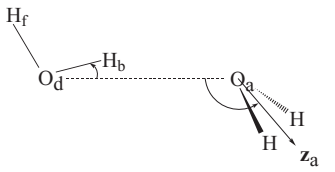

FIG. 1. Equilibrium geometry of the water dimer and naming conventions used in the text: *d* means the donor molecule, and *a* the acceptor one; H_f and H_b correspond, respectively, to the free and bound hydrogens in the donor molecule.

each monomer. These two sets of coordinates are not independent as the Euler angles $\mathbf{\Omega}^X$ that determine the orientation of monomer X with respect to a dimer frame depend on the embedding of the monomer frame in the (vibrationally distorted) monomer. The SAPT-5s′*f*IR potential depends only on the Cartesian coordinates of all atoms which uniquely define the 12D geometry of the system. This 12D geometry can then be represented by a set of inter- and intra-monomer coordinates based on arbitrary embedding. Thus, we first associate with any 12D distorted geometry ($\mathbf{d}$), specified by Cartesian coordinates of all atoms, the set ($\mathbf{q}^A, \mathbf{q}^B, \mathbf{Q}$) based on some assumed embedding. The undistorted geometry is then ($\mathbf{u}$) ≡ ($\mathbf{q}_{\rm ref}, \mathbf{q}_{\rm ref}, \mathbf{Q}$), where $\mathbf{q}_{\rm ref}$ corresponds to the vibrationally averaged geometry mentioned before. Equation (5) can thus be rewritten more explicitly as

$$V^{(2)}_{\text{CCpol-8s}f}(\mathbf{q}^A, \mathbf{q}^B, \mathbf{Q}) = V^{(2)}_{\text{CCpol-8s}}(\mathbf{Q}) + V^{(2)}_{\text{SAPT-5s}'f\text{IR}}(\mathbf{q}^A, \mathbf{q}^B, \mathbf{Q}) - V^{(2)}_{\text{SAPT-5s}'}(\mathbf{Q}). \quad (6)$$

Note that $V^{(2)}_{\text{SAPT-5s}'}(\mathbf{Q}) = V^{(2)}_{\text{SAPT-5s}'f\text{IR}}(\mathbf{q}_{\rm ref}, \mathbf{q}_{\rm ref}, \mathbf{Q})$. As the above definition refers to the two-body term, it must be supplemented by the one-body terms $V^{(1)}(\mathbf{q}^X)$ to obtain the full potential energy of the water dimer

$$V_{\text{CCpol-8s}f}(\mathbf{q}^A, \mathbf{q}^B, \mathbf{Q}) = V^{(1)}(\mathbf{q}^A) + V^{(1)}(\mathbf{q}^B) + V^{(2)}_{\text{CCpol-8s}f}(\mathbf{q}^A, \mathbf{q}^B, \mathbf{Q}). \quad (7)$$

For the one-body terms, we used the spectroscopically accurate water PJT2 potential of Polyansky *et al.*[36] It should be noted that these one-body terms were already included in the fitting of the flexible-monomer SAPT-5s′*f*IR potential to the set of *ab initio* points.

Table I shows that this new flexible-monomer potential gives significantly better characteristics of the global minimum than SAPT-5s′*f*IR. In particular, the 5.2% error in the binding energy D_e is reduced to zero and the errors of intermonomer coordinates are all below 1%.

III. VRT LEVELS FROM A FLEXIBLE-MONOMER POTENTIAL

In this section, we first define the coordinates used to describe the fully flexible water dimer and the resulting Hamilton operator. We then explain the adiabatic decoupling between the fast (intramolecular) and slow (intermolecular) modes, and the different approximations which can be invoked depending on the level of accuracy needed. In particular, we will consider how the time-consuming calculation of the adiabatic potential can be drastically accelerated by neglecting a part of the potential coupling between the intramolecular modes located on different monomers. We then discuss two limiting cases for the definition of intramolecular excitations of the two monomers to account for the breakdown of the adiabatic separation between the intramolecular modes on different monomers. Finally, it is shown that this adiabatic scheme allows us to recast the calculation into a pseudo-rigid monomer one using an adiabatic potential energy surface, except for the rotational constants which depend on the intermolecular geometry.

A. Full flexible-monomer Hamiltonian

As formulated in a previous paper,[22] the exact Hamiltonian for the fully flexible water dimer is

$$\hat{H} = -\frac{\hbar^2}{2\mu_{AB}\mathcal{R}}\frac{\partial^2}{\partial\mathcal{R}^2}\mathcal{R} + \hat{T}^A_{VR} + \hat{T}^B_{VR} + V(\mathbf{q}^A, \mathbf{q}^B, \mathbf{Q}) + \frac{1}{2\mu_{AB}\mathcal{R}^2}\{\hat{\boldsymbol{J}}^2 + \hat{\boldsymbol{j}}^2_{AB} - 2\hat{\boldsymbol{j}}_{AB}\cdot\hat{\boldsymbol{J}}\}, \quad (8)$$

where $\hat{\boldsymbol{j}}_{AB} = \hat{\boldsymbol{j}}_A + \hat{\boldsymbol{j}}_B$ with $\hat{\boldsymbol{j}}_A$ and $\hat{\boldsymbol{j}}_B$ the internal rotation angular momenta of the monomers, $\hat{\boldsymbol{J}} = \hat{\boldsymbol{j}}_{AB} + \hat{\mathbf{L}}$ is the total angular momentum with $\hat{\mathbf{L}}$ being the end-over-end angular momentum of the monomers' centers of mass and μ_{AB} is the reduced mass of the dimer. The operator $\hat{T}^X_{VR}$ represents the vibration-rotation kinetic energy operator (KEO) of monomer X, to be specified in Sec. III C. In order to proceed with the derivations, we re-express this KEO in matrix form[37] (suppressing the X label)

$$\hat{T}_{VR} = \frac{1}{2}[\hat{\boldsymbol{p}}^\dagger\ \hat{\boldsymbol{j}}^\dagger]\begin{pmatrix}\mathbf{\Sigma} & \boldsymbol{\sigma}\\ \boldsymbol{\sigma}^t & \mathbf{\Gamma}\end{pmatrix}\begin{bmatrix}\hat{\boldsymbol{p}}\\ \hat{\boldsymbol{j}}\end{bmatrix}, \quad (9)$$

with $\hat{\boldsymbol{p}} = (\hat{p}_1, \hat{p}_2, \hat{p}_3)$ being the momenta conjugate to the internal coordinates (q_1, q_2, q_3) and $\hat{\boldsymbol{j}} = (\hat{j}_x, \hat{j}_y, \hat{j}_z)$ the rotational angular momentum components. The matrices $\mathbf{\Sigma}$, $\mathbf{\Gamma}$, and $\boldsymbol{\sigma}$ are defined in Sec. III C.

An exact quantum calculation explicitly treating these 12 internal degrees of freedom would probably be possible nowadays, due to the huge computing power of massively parallel machines. However, one can resort to an *adiabatic* separation between the "fast" intramolecular coordinates {$\mathbf{q}^A$, $\mathbf{q}^B$} and the "slow" intermolecular coordinates $\mathbf{Q}$, as applied before by Klopper, Quack, and Suhm[38,39] in a [4 + 2]D treatment of the HF dimer, and more recently by one of us and co-workers for the water dimer.[22]

B. Adiabatic approximation

To define here such a [6+6]D formulation, i.e., to decouple the intramolecular coordinates from the intermolecular ones, we make two basic approximations:

(i) we set the intramolecular vibration-rotation coupling matrix $\boldsymbol{\sigma}$ to zero, so that

$$\hat{T}_{VR} \simeq \hat{T}^{(\text{ad})}_{VR} = \hat{T}^{(\text{ad})}_{V} + \hat{T}^{(\text{ad})}_{R}, \quad (10)$$

which will be justified later on. This allows a partitioning of the total Hamiltonian according to

$$\hat{H}^{(\text{ad})} = \hat{H}_{\text{inter}} + \hat{H}_{\text{intra}}(\mathbf{Q}), \quad (11)$$

with

$$\hat{H}_{\text{inter}} = \hat{T}_{\mathcal{R}} + \hat{T}^{A(\text{ad})}_{R} + \hat{T}^{B(\text{ad})}_{R} + \hat{T}_{\text{CC}}, \quad (12)$$

$$\hat{H}_{\rm intra}(\mathbf{Q}) = \hat{T}_V^{A({\rm ad})} + \hat{T}_V^{B({\rm ad})} + V(\mathbf{q}^A, \mathbf{q}^B; \mathbf{Q}), \qquad (13)$$

where $\hat{T}_{\mathcal{R}}$ stands for the first term of Eq. (8) and $\hat{T}_{\rm CC}$ (centrifugal and Coriolis coupling) for the last term in this equation.

(ii) the **Q**-dependence of the intramolecular modes is treated in the "clamped **Q**" approximation, nonadiabatic coupling terms are neglected. The calculations of the intramolecular modes proceed as presented below.

C. 6D intramolecular calculations

The intramolecular (adiabatic) eigenfunctions $\Phi_{\mathbf{N}}(\mathbf{q}^A, \mathbf{q}^B; \mathbf{Q})$ at fixed **Q** are obtained from the eigenvalue problem

$$\left\{\hat{T}_V^{A({\rm ad})} + \hat{T}_V^{B({\rm ad})} + V(\mathbf{q}^A, \mathbf{q}^B, \mathbf{Q})\right\}\Phi_{\mathbf{N}}(\mathbf{q}^A, \mathbf{q}^B; \mathbf{Q})$$
$$= V_{\mathbf{N}}^{({\rm ad})}(\mathbf{Q})\Phi_{\mathbf{N}}(\mathbf{q}^A, \mathbf{q}^B; \mathbf{Q}), \qquad (14)$$

with the intramolecular Hamiltonian of Eq. (13). The subscript **N** is a composite index representing the six vibrational quantum numbers associated with the two monomers, as will be discussed in Sec. III D.

For efficient convergence, we express the $\hat{T}_V^{X({\rm ad})}$ operators in terms of Radau's coordinates (r_1, r_2, β) (Ref. 40)

$$\hat{T}_V^{({\rm ad})} = \frac{1}{2}\hat{\boldsymbol{p}}^\dagger\,\boldsymbol{\Sigma}\,\hat{\boldsymbol{p}}$$
$$= \frac{1}{2}[\hat{p}_{r_1}^\dagger, \hat{p}_{r_2}^\dagger, \hat{p}_\beta^\dagger]\begin{pmatrix} \frac{1}{m_H} & 0 & 0 \\ 0 & \frac{1}{m_H} & 0 \\ 0 & 0 & \frac{1}{m_H r_1^2} + \frac{1}{m_H r_2^2} \end{pmatrix}\begin{bmatrix} \hat{p}_{r_1} \\ \hat{p}_{r_2} \\ \hat{p}_\beta \end{bmatrix}, \qquad (15)$$

where m_H is the mass of hydrogen atom which are ideally suited to the H_2O molecule as shown by Bačić *et al.*[41] We use the *f*-embedding formulation of Wei and Carrington,[42,43] with the value of the *f* parameter equal to 1, i.e., choosing the *z* axis of each monomer frame as the vector that bisects the angle between the two Radau vectors. This results in a **Γ** matrix given by

$$\boldsymbol{\Gamma} = \frac{1}{2m_H}\begin{pmatrix} \frac{1}{2}\left[\frac{1}{r_1^2} + \frac{1}{r_2^2}\right] & 0 & 0 \\ 0 & \frac{1}{1-c}\left[\frac{1}{r_1^2} + \frac{1}{r_2^2}\right] & \frac{1}{\sqrt{1-c^2}}\left[\frac{1}{r_2^2} - \frac{1}{r_1^2}\right] \\ 0 & \frac{1}{\sqrt{1-c^2}}\left[\frac{1}{r_2^2} - \frac{1}{r_1^2}\right] & \frac{1}{1+c}\left[\frac{1}{r_1^2} + \frac{1}{r_2^2}\right] \end{pmatrix}, \qquad (16)$$

where $c = \cos\beta$. The resulting Coriolis matrix $\boldsymbol{\sigma}$ entering Eq. (9) has only zero elements except for

$$\sigma_{\beta x} = \sigma_{x\beta} = \frac{1}{2m_H}\sqrt{1-c^2}\left[\frac{1}{r_1^2} - \frac{1}{r_2^2}\right], \qquad (17)$$

which vanish at equilibrium ($r_1 = r_2$), and stay very small except for highly distorted monomer geometries. In the work presented here, this term was neglected, which allowed for the decoupling of the intermolecular calculations from the intramolecular ones. Actually, this intramolecular Coriolis coupling gives rise to the terms

$$\hat{p}_\beta^\dagger\,\sigma_{\beta x}\,\hat{j}_x + \hat{j}_x^\dagger\,\sigma_{x\beta}\,\hat{p}_\beta,$$

which would lead to a correction that vanishes in first-order perturbation theory. This is easily shown by expressing $\hat{j}_x$ in terms of ladder operators $\hat{j}_x = \frac{1}{2}(\hat{j}_+ + \hat{j}_-)$ that have vanishing diagonal matrix elements in the asymmetric rotor eigenfunction basis of the H_2O monomers (see Sec. III E).

The adiabatic intermolecular potential $V_{\mathbf{N}}^{({\rm ad})}(\mathbf{Q})$ results from a six-dimensional calculation of Eq. (14), to be performed for every six-dimensional intermolecular geometry ($\simeq 10^6$ **Q**-points). In order to make these calculations efficient, we used the following two-step procedure at each geometry **Q**:

(i) We first optimize the intramolecular geometry $(\mathbf{q}^A_{\rm opt}, \mathbf{q}^B_{\rm opt})$ for a given geometry **Q**, so that

$$\left.\frac{\partial V(\mathbf{q}^A, \mathbf{q}^B, \mathbf{Q})}{\partial \mathbf{q}^X}\right|_{\mathbf{q}^X_{\rm opt}} = \mathbf{0} \qquad (X = A, B). \qquad (18)$$

We use the Powell method[44] which does not require analytic energy derivatives. The associated potential energy is $V_{\rm opt}(\mathbf{Q}) = V(\mathbf{q}^A_{\rm opt}, \mathbf{q}^B_{\rm opt}, \mathbf{Q})$.

(ii) We then expand the intramolecular potential around the minimum

$$V(\mathbf{q}^A, \mathbf{q}^B; \mathbf{Q}) = V(\mathbf{q}^A_{\rm opt}, \mathbf{q}^B_{\rm opt}; \mathbf{Q}) \qquad (\equiv V_{\rm opt}(\mathbf{Q}))$$
$$+ V(\mathbf{q}^A, \mathbf{q}^B_{\rm opt}; \mathbf{Q}) - V_{\rm opt}(\mathbf{Q}) \qquad (\equiv V^A(\mathbf{q}^A; \mathbf{Q}))$$
$$+ V(\mathbf{q}^A_{\rm opt}, \mathbf{q}^B; \mathbf{Q}) - V_{\rm opt}(\mathbf{Q}) \qquad (\equiv V^B(\mathbf{q}^B; \mathbf{Q}))$$
$$+ V(\mathbf{q}^A, \mathbf{q}^B; \mathbf{Q}) - V^A(\mathbf{q}^A; \mathbf{Q}) - V^B(\mathbf{q}^B; \mathbf{Q}) - V_{\rm opt}(\mathbf{Q}) \qquad (\equiv V^{AB}(\mathbf{q}^A, \mathbf{q}^B; \mathbf{Q})), \qquad (19)$$

which allows one to define single-monomer terms $V^X(\mathbf{q}^X;\mathbf{Q})$ at fixed optimized geometry of the other monomer and a residual coupling term $V^{AB}(\mathbf{q}^A,\mathbf{q}^B;\mathbf{Q})$ between the two monomers.

(iii) The vibrational states of monomer X are *exactly* computed in the field of the other monomer frozen at its optimized geometry, by means of a sequential truncation-reduction scheme[45,46]

$$\left\{\hat{T}_V^{X(\mathrm{ad})} + V^X(\mathbf{q}^X;\mathbf{Q})\right\}\varphi_{\mathbf{n}_X}(\mathbf{q}^X;\mathbf{Q}) = E^X_{\mathbf{n}_X}(\mathbf{Q})\varphi_{\mathbf{n}_X}(\mathbf{q}^X;\mathbf{Q}). \tag{20}$$

The eigenvalue $E^X_{\mathbf{n}_X}(\mathbf{Q})$ represents the energy of mode $\mathbf{n}_X$ with respect to the instantaneous energy minimum. The six-dimensional zero-order intramolecular states $\Phi^{(0)}_{\mathbf{N}}(\mathbf{q}^A,\mathbf{q}^B;\mathbf{Q})$ are then defined as

$$\Phi^{(0)}_{\mathbf{N}}(\mathbf{q}^A,\mathbf{q}^B;\mathbf{Q}) = \varphi_{\mathbf{n}_A}(\mathbf{q}^A;\mathbf{Q})\,\varphi_{\mathbf{n}_B}(\mathbf{q}^B;\mathbf{Q}), \tag{21}$$

with associated energies

$$V^{[3+3]\mathrm{D}}_{\mathbf{N}}(\mathbf{Q}) = V_{\mathrm{opt}}(\mathbf{Q}) + E^A_{\mathbf{n}_A}(\mathbf{Q}) + E^B_{\mathbf{n}_B}(\mathbf{Q}) - 2E_0^\infty, \tag{22}$$

where E_0^∞ is the zero-point energy of an isolated monomer. This approach corresponds to the [3+3]D adiabatic formulation in which one ignores the potential coupling between intramolecular modes. The ground state energy $V_{\mathbf{0}}^{[3+3]\mathrm{D}}(\mathbf{Q})$ reflects the change in the zero-point energies of both monomers when the intermolecular geometry $\mathbf{Q}$ varies. With this definition, the dissociation limit $V_{\mathbf{0}}^{[3+3]\mathrm{D}}(\mathcal{R}\to\infty)$ equals zero provided that $\lim_{\mathcal{R}\to\infty} V_{\mathrm{opt}}(\mathbf{Q}) = 0$.

(iv) The remaining term $V^{AB}(\mathbf{q}^A,\mathbf{q}^B;\mathbf{Q})$ can then be taken into account either by perturbation theory

$$V^{6\mathrm{D}p}_{\mathbf{N}}(\mathbf{Q}) = V_{\mathrm{opt}}(\mathbf{Q}) + E^A_{\mathbf{n}_A}(\mathbf{Q}) + E^B_{\mathbf{n}_B}(\mathbf{Q}) - 2E_0^\infty + \langle\varphi^A_{\mathbf{n}_A}(\mathbf{Q})\varphi^B_{\mathbf{n}_B}(\mathbf{Q})|V^{AB}|\varphi^A_{\mathbf{n}_A}(\mathbf{Q})\varphi^B_{\mathbf{n}_B}(\mathbf{Q})\rangle, \tag{23}$$

which we call the 6Dp adiabatic formulation, or within a full variational treatment in which the potentials $V^{6\mathrm{D}}_{\mathbf{N}}(\mathbf{Q})$ are defined as the eigenvalues of the Hamiltonian matrix

$$\hat{H}_{\mathbf{n}_A'\mathbf{n}_B';\mathbf{n}_A\mathbf{n}_B} = \left[V_{\mathrm{opt}}(\mathbf{Q}) + E^A_{\mathbf{n}_A}(\mathbf{Q}) + E^B_{\mathbf{n}_B}(\mathbf{Q}) - 2E_0^\infty\right]\delta_{\mathbf{n}_A'\mathbf{n}_A}\delta_{\mathbf{n}_B'\mathbf{n}_B} + \langle\varphi^A_{\mathbf{n}_A'}(\mathbf{Q})\varphi^B_{\mathbf{n}_B'}(\mathbf{Q})|V^{AB}|\varphi^A_{\mathbf{n}_A}(\mathbf{Q})\varphi^B_{\mathbf{n}_B}(\mathbf{Q})\rangle, \tag{24}$$

which is named the 6D adiabatic formulation.

These three different definitions of the adiabatic potential will be compared further on.

D. Excited intramolecular states

In our [6+6]D adiabatic model for the vibrational ground state of the monomers, the 6D adiabatic intermolecular potential has eight equivalent minima. Each of these minima corresponds to a hydrogen-bonded structure in which one of the monomers is the donor in the hydrogen bond and the other monomer is the acceptor. In four of the minima, monomer A is the donor and B the acceptor, in the other four minima the monomers are interchanged, so that B is the donor and A the acceptor. The intermolecular VRT states calculated on the ground state potential also correspond to hydrogen-bonded structures; they are adapted to the irreducible representations (irreps) of the full permutation-inversion group G_{16}. The states that carry the one-dimensional irreps of G_{16} are either symmetric or antisymmetric with respect to the monomer interchange operator P_{AB}, which leads to a small ($\approx$1 cm^{-1}) interchange tunneling splitting of the intermolecular rovibrational levels. The two components of the states that carry the two-dimensional G_{16} irreps are interchanged by the action of P_{AB} and the corresponding energy levels are not split by interchange tunneling.

If one of the monomers is vibrationally excited, the situation is more complicated. If the excitation is localized on one of the monomers, say A, the corresponding adiabatic intermolecular potential is no longer symmetric under donor-acceptor interchange P_{AB}. An equivalent adiabatic state exists with monomer B excited, which is not symmetric under P_{AB} either, but which may be obtained from the adiabatic state in which A is excited by acting on it with P_{AB}. The interchange tunneling splitting in the monomer excited state can be calculated from a two-state model in which the two equivalent adiabatic potentials and the non-adiabatic coupling are included, as it was done, for example, by Fraser.[47] The excited state interchange tunneling splitting is smaller by an order of magnitude than the corresponding ground state splitting[5] because the monomer excitation is localized either on the donor or on the acceptor, and donor-acceptor interchange also involves hopping of the excitation between the monomers A and B. So, it is clear that our adiabatic [6+6]D model would have to be extended to compute reliable values of the excited state interchange tunneling splitting. This is not a goal of the present paper, however. Here, we perform monomer excited state calculations to obtain the infrared frequency shifts of the monomer vibrations in the dimer. In a previous paper,[34] two of us discussed and applied two approximate methods to do this, while maintaining the [6+6]D adiabatic model.

(i) One option is to identify the donor (D) and the acceptor (A) monomers at each intermolecular geometry $\mathbf{Q}$, and to define donor- or acceptor-excited adiabatic potentials. The acceptor can, for example, be identified as the monomer displaying the shortest $d_{\mathrm{O}\cdots\mathrm{H}}$ distance between its oxygen atom and a hydrogen atom located on the other monomer. Such a definition retains the full G_{16} symmetry of the adiabatic intermolecular potentials, and we will therefore call it the G_{16} model. It implies that upon donor-acceptor interchange (which corresponds to bringing the complex from one minimum to an equivalent one) the excitation energy simultaneously migrates from one monomer to the other. The interchange tunneling splitting that would result from this model for the excited state would be roughly of the same size as the ground state interchange tunneling splitting, in contrast with high-resolution spectra[5] which show that the excited state tunneling splitting is reduced by one

order of magnitude with respect to the ground state splitting.

(ii) A second possibility is to stipulate that, whatever is the intermolecular geometry $\mathbf{Q}$, the excitation energy stays on the same monomer, say A. In that case, the excitation does not migrate upon donor-acceptor interchange. The symmetry of the adiabatic potentials is broken because the minima at geometries $\mathbf{Q}_{\rm eq}$ differ slightly in energy from those at $P_{AB}\mathbf{Q}_{\rm eq}$. As the interchange P_{AB} is no longer a symmetry operation, the G_{16} symmetry of the intermolecular VRT states is lost and one must use the subgroup G_8 instead. If this scheme, which we call the G_8 model, were used to compute excited state interchange tunneling splittings, the resulting splittings would be too small.

In Sec. IV, we will present results corresponding to these two extreme possibilities, and show that they produce nearly identical infrared frequency shifts of the monomer vibrations in the water dimer.

E. 6D intermolecular calculations

The full dimer wave function $\Psi_{\mathbf{N}}(\mathbf{q}^A, \mathbf{q}^B, \mathbf{Q})$ is a solution of the equation

$$(\hat{H}_{\rm inter} + \hat{H}_{\rm intra}(\mathbf{Q}))\Psi_{\mathbf{N}} = \mathcal{E}^{\mathbf{N}}\Psi_{\mathbf{N}}, \tag{25}$$

with the operators $\hat{H}_{\rm inter}$ and $\hat{H}_{\rm intra}(\mathbf{Q})$ defined in Eqs. (12) and (13). Within the adiabatic approximation, the full dimer wave function is written as

$$\Psi_{\mathbf{N}}(\mathbf{q}^A, \mathbf{q}^B, \mathbf{Q}) = \Phi_{\mathbf{N}}(\mathbf{q}^A, \mathbf{q}^B; \mathbf{Q})\, \psi^{\mathbf{N}}(\mathbf{Q}). \tag{26}$$

Neglecting all non-adiabatic coupling terms, the Schrödinger equation to be solved in the coordinates $\{\mathbf{q}^{\mathbf{A}}, \mathbf{q}^{\mathbf{B}}, \mathbf{Q}\}$ thus reads as

$$\begin{aligned}\left\{\hat{T}_{\mathcal{R}} + \hat{T}_R^{A(\rm ad)} + \hat{T}_R^{B(\rm ad)} + \hat{T}_{CC} + V_{\mathbf{N}}^{(\rm ad)}(\mathbf{Q})\right\}\Phi_{\mathbf{N}}\,\psi^{\mathbf{N}} \\ = \mathcal{E}^{\mathbf{N}}\Phi_{\mathbf{N}}\,\psi^{\mathbf{N}}.\end{aligned} \tag{27}$$

The operators that differentiate with respect to the intermolecular coordinates $\mathbf{Q}$ act only on $\psi^{\mathbf{N}}$ and not on the function $\Phi_{\mathbf{N}}$, as implied by the adiabatic approximation. The adiabatic potential $V_{\mathbf{N}}^{(\rm ad)}(\mathbf{Q})$ in this equation was obtained by solving the eigenvalue problem, Eq. (14), in the intramolecular coordinates $\mathbf{q}^A$, $\mathbf{q}^B$ with clamped $\mathbf{Q}$. Projecting Eq. (27) onto the adiabatic eigenfunction $\Phi_{\mathbf{N}}(\mathbf{q}^A, \mathbf{q}^B; \mathbf{Q})$, one obtains the *intermolecular* equation

$$\left\{\hat{T}_{\mathcal{R}} + \hat{T}_R^{A(\mathbf{N})} + \hat{T}_R^{B(\mathbf{N})} + \hat{T}_{CC} + V_{\mathbf{N}}^{(\rm ad)}(\mathbf{Q})\right\}\psi^{\mathbf{N}}(\mathbf{Q}) = \mathcal{E}^{\mathbf{N}}\psi^{\mathbf{N}}(\mathbf{Q}). \tag{28}$$

The notation $\hat{T}_R^{X(\mathbf{N})}$, with the operators $\hat{T}_R^{X(\rm ad)}$ defined in Eqs. (9) and (10), implies averaging over the adiabatic monomer states $\Phi_{\mathbf{N}}(\mathbf{q}^A, \mathbf{q}^B; \mathbf{Q})$, i.e., integration over the monomer coordinates $\mathbf{q} \equiv \{\mathbf{q}^A, \mathbf{q}^B\}$

$$\hat{T}_R^{X(\mathbf{N})} = \frac{1}{2}\hat{\boldsymbol{\jmath}}^{X\dagger}\,\langle\Phi_{\mathbf{N}}|\boldsymbol{\Gamma}^X|\Phi_{\mathbf{N}}\rangle_{\mathbf{q}}\,\hat{\boldsymbol{\jmath}}^X \equiv \frac{1}{2}\hat{\boldsymbol{\jmath}}^{X\dagger}\,\boldsymbol{\Gamma}^{X(\mathbf{N})}\,\hat{\boldsymbol{\jmath}}^X. \tag{29}$$

In Sec. IV, we will also present calculations in which this term was obtained without averaging, but instead evaluated for the optimized intramolecular coordinates $\mathbf{q}_{\rm opt}$, see Eq. (18),

$$\hat{T}_R^{X(\rm opt)} = \frac{1}{2}\hat{\boldsymbol{\jmath}}^{X\dagger}\,\boldsymbol{\Gamma}^{X(\rm opt)}\,\hat{\boldsymbol{\jmath}}^X, \tag{30}$$

with $\boldsymbol{\Gamma}^{X(\rm opt)} = \boldsymbol{\Gamma}^X(\mathbf{q}^X_{\rm opt})$. Such term is denoted as *"optimized"* in contrast to the *"averaged"* version of Eq. (29). In both cases, the operator $\hat{T}_R$ contains off-diagonal terms, cf. Eqs. (9) and (16)

$$\Gamma_{yz}\{\hat{\jmath}_y^\dagger\,\hat{\jmath}_z + \hat{\jmath}_z^\dagger\,\hat{\jmath}_y\}. \tag{31}$$

These terms will be neglected as Γ_{yz} is much smaller than the diagonal elements in Eq. (16) when the monomer geometries are not too strongly distorted and $r_1 \approx r_2$. Moreover, their contribution vanishes in first-order perturbation theory due to the fact that $\hat{\jmath}_y$ only contains step-up and step-down operators.

Equation (28) formally corresponds to the formulation of Brocks *et al.*[48] for rigid monomers, but it uses an adiabatic potential which reflects the variation of the monomer zero-point energies as a function of the intermolecular geometry $\mathbf{Q}$. A second, important difference stems from the $\mathbf{Q}$-dependence of the rotational constant matrices $\boldsymbol{\Gamma}^{X(\mathbf{N})}$ of the monomers. The coordinates $(r_1, r_2, \cos\beta)$ entering Eq. (16) correspond to either the optimized values $\mathbf{q}_{\rm opt}(\mathbf{Q})$ given by Eq. (18) or they are averaged over $\mathbf{Q}$-dependent adiabatic monomer eigenfunctions as shown in Eq. (29). Explicitly handling these $\mathbf{Q}$-dependent terms makes the energy levels calculation about one order of magnitude more expensive than in the rigid case. Therefore, we have investigated the approximation of making the $\boldsymbol{\Gamma}^{X(\mathbf{N})}$ (or $\boldsymbol{\Gamma}^{X(\rm opt)}$) matrices independent of the Euler angles $\boldsymbol{\Omega}^A$ and $\boldsymbol{\Omega}^B$ through the averaging procedure

$$\begin{aligned}\widetilde{\boldsymbol{\Gamma}}^{X(\mathbf{N})}(\mathcal{R}) = \int d\boldsymbol{\Omega}^A \int d\boldsymbol{\Omega}^B \boldsymbol{\Gamma}^{X(\mathbf{N})}(\mathcal{R}, \boldsymbol{\Omega}^A, \boldsymbol{\Omega}^B) \\ \times \exp\left(-\alpha\left[V_{\mathbf{N}}^{(\rm ad)}(\mathcal{R}, \boldsymbol{\Omega}^A, \boldsymbol{\Omega}^B) - V_{\rm min}\right]\right),\end{aligned} \tag{32}$$

while explicitly retaining the $\mathcal{R}$-dependence. In Eq. (32), $V_{\rm min}$ is the minimum value of the potential and α is some constant ($\approx 10^2$ Hartree^{-1}). This approximation allows us to recast the fully flexible formulation into a rigid one, except for the rotational matrices $\widetilde{\boldsymbol{\Gamma}}^{X(\mathbf{N})}$ which only depend on the separation $\mathcal{R}$. Within this averaging approximation, which yields

$$\widetilde{T}_R^{X(\mathbf{N})} = \frac{1}{2}\hat{\boldsymbol{\jmath}}^{X\dagger}\,\widetilde{\boldsymbol{\Gamma}}^{X(\mathbf{N})}(\mathcal{R})\,\hat{\boldsymbol{\jmath}}^X, \tag{33}$$

we will consider the two possibilities of either ignoring the angular dependence of the $\boldsymbol{\Gamma}^{X(\mathbf{N})}$ matrices

$$\left\{\hat{T}_{\mathcal{R}} + \widetilde{T}_R^{A(\mathbf{N})} + \widetilde{T}_R^{B(\mathbf{N})} + \hat{T}_{CC} + V_{\mathbf{N}}^{(\rm ad)}(\mathbf{Q})\right\}\widetilde{\psi}^{\mathbf{N}}_{\mathbf{n}}(\mathbf{Q}) = \widetilde{\mathcal{E}}^{\mathbf{N}}_{\mathbf{n}}\widetilde{\psi}^{\mathbf{N}}_{\mathbf{n}}(\mathbf{Q}) \tag{34}$$

or subsequently retrieving this dependence with

$$\Delta\boldsymbol{\Gamma}^{X(\mathbf{N})}(\mathbf{Q}) = \boldsymbol{\Gamma}^{X(\mathbf{N})}(\mathbf{Q}) - \widetilde{\boldsymbol{\Gamma}}^{X(\mathbf{N})}(\mathcal{R}) \tag{35}$$

by first order perturbation theory

$$\Delta\widetilde{\mathcal{E}}^{\mathbf{N}}_{\mathbf{n}} = \frac{1}{2}\langle\widetilde{\psi}^{\mathbf{N}}_{\mathbf{n}}|\hat{\boldsymbol{\jmath}}^{A\dagger}\,\Delta\boldsymbol{\Gamma}^{A(\mathbf{N})}\,\hat{\boldsymbol{\jmath}}^A + \hat{\boldsymbol{\jmath}}^{B\dagger}\,\Delta\boldsymbol{\Gamma}^{B(\mathbf{N})}\,\hat{\boldsymbol{\jmath}}^B|\widetilde{\psi}^{\mathbf{N}}_{\mathbf{n}}\rangle. \tag{36}$$

We will show in Sec. IV that this latter correction essentially gives the exact transition energies obtained from Eq. (28).

A detailed description of the implementation of the calculation of the intermolecular VRT states has been given previously.[12,49] For the sake of clarity, we briefly recall it. The intermolecular KEO of Eq. (28) leads to simple matrix elements in the overall basis set

$$\mathcal{B} = \{|n\rangle\} \otimes \{|j_A, k_A, m_A\rangle\} \otimes \{|j_B, k_B, m_B\rangle\} \otimes \{|J, K, M\rangle\} \quad (m_A + m_B = K), \tag{37}$$

where $\{|n\rangle\}$ is an appropriate basis in the interfragment distance coordinate $\mathcal{R}$, the Wigner functions $\langle \mathbf{\Omega}|j,k,m\rangle = \sqrt{(2j+1)/8\pi^2}\, D^{j*}_{mk}(\mathbf{\Omega})$ form a basis for the rotation of each monomer with the Euler angles $\mathbf{\Omega}^X = \{\varphi^X, \theta^X, \chi^X\}$, and $\{|J,K,M\rangle\}$ is the Wigner basis associated with the overall rotation of the complex. The basis $\mathcal{B}$ can be projected onto the different irreps Γ of the molecular symmetry group G_{16} (or G_8) used to label the energy levels[50]

$$\mathcal{B} = \bigoplus_{\Gamma} \{|n\rangle \otimes |\boldsymbol{\nu}; \Gamma\rangle\},$$

where $\boldsymbol{\nu}$ stands for the combination of all angular quantum numbers. The most compact representation for the adiabatic potential energy $V^{(\mathrm{ad})}_{\mathbf{N}}(\mathcal{R}, \mathbf{\Omega}^A, \mathbf{\Omega}^B)$ is the six-dimensional direct-product grid $\{\boldsymbol{\varphi} \times \boldsymbol{\chi}^A \times \boldsymbol{\chi}^B \times \boldsymbol{\theta}^A \times \boldsymbol{\theta}^B \times \boldsymbol{\mathcal{R}}\}$, where the symbols $\boldsymbol{\varphi}$, etc., denote the grids in the respective coordinates and the coordinate $\varphi = \varphi^A - \varphi^B$. This grid is *restricted* to points where the potential energy is lower than some threshold value $V_{\max}$, and only non-symmetry-equivalent points are computed, which typically corresponds to a dimension of about 10^6. As the six-dimensional intramolecular eigenvalue problem has to be solved for each point of this grid, this is an expensive step of the whole calculation. It is straightforwardly parallelized by means of the Open MP protocol. More specifically, the inner do-loop running over the φ, χ^A, and χ^B grid points was declared to run in parallel. On a 12-core processor, a speed up factor of 5.9 was obtained, close to the best performance expected due to the limited size of the common cache memory. Energy levels are computed from an iterative Lanczos procedure,[51] parallelized on the outer do-loop running over the radial basis set index. A similar speed up factor of 6.8 was obtained for this step. When needed, intermolecular eigenvectors $|\psi^{\mathbf{N}}_\alpha\rangle$ were computed afterwards from the previously stored Lanczos vectors $\{|u_n\rangle\}$

$$|\psi^{\mathbf{N}}_\alpha\rangle = \sum_n T_{n\alpha}|u_n\rangle, \tag{38}$$

where $\mathbf{T}$ corresponds to the eigenvector matrix resulting from the diagonalization of the tridiagonal Hamiltonian matrix built by the Lanczos scheme. Transformations between the spectral and grid representations,[12,49] as required to act with the potential energy operator on the successive Lanczos vectors, are performed by means of a six-dimensional pseudo-spectral scheme involving a three-dimensional fast Fourier transform. Depending on the method, [3+3]D, 6Dp, or 6D, used to compute the adiabatic potential, the whole calculation will be termed [6+[3+3]]D, [6D+6Dp] or [6+6]D, respectively, as the intermolecular calculation is effectively six-dimensional.

TABLE II. IR excitation frequencies (in cm^{-1}), calculated for the isolated monomer and the water dimer equilibrium geometry, as a function of the intramolecular basis set selected: b denotes the bend mode, ss the symmetric stretch, and as the antisymmetric stretch. The upper part of the table refers to the isolated monomer, the lower one to the dimer equilibrium geometry: O–$H_b[D]$ and O–$H_f[D]$ correspond to the two donor OH stretches (see Fig. 1), $zpe[X]$ to the zero-point energy of monomer X.

IR excitation	Basis I	Basis II	Basis III	Expt.
H_2O				
b	1594.68	1594.67	1594.67	1594.7
ss	3658.29	3657.23	3657.19	3657.1
as	3755.99	3755.87	3755.86	3756.0
$(H_2O)_2$				
$b[D]$	1609.0	1609.0	1609.0	
O–$H_b[D]$	3547.6	3543.9	3543.4	
O–$H_f[D]$	3738.4	3737.9	3737.9	
$zpe[D]$	4595.87	4595.82	4595.82	
$b[A]$	1597.3	1597.3	1597.3	
$ss[A]$	3658.6	3657.6	3657.6	
$as[A]$	3750.5	3750.4	3750.4	
$zpe[A]$	4630.86	4630.85	4630.85	

IV. RESULTS

In this section, we present the results obtained from the new potential for the MW and far IR spectra, and the frequency shifts of the monomer vibrations observed in IR spectra of the $(H_2O)_2$ dimer, and compare with available experimental data. We also present results for the $(D_2O)_2$ dimer, for which accurate VRT spectra are available as well. First, we describe the basis set specifications used in the calculations.

A. Specification of basis sets and convergence tests

1. Intramolecular basis set

The intramolecular calculations used a local biharmonic basis set $\{H_m(r_1;\beta_s)\}\otimes\{H_n(r_2;\beta_s)\}$ on each monomer which was contracted at each sampled value of the grid for the Radau angle β. The three-dimensional resulting eigenvalues and eigenvectors are then obtained by means of a sequential truncation-reduction scheme.[45,46] Two different monomer intramolecular bases were considered in the calculations: the first basis (I) consisted of 7 harmonic functions along each radius r_i and 19 sampled angles β_s. For the second basis (II), these numbers were increased to 9 and 25, respectively. Furthermore, for convergence checking only, we also performed test calculations with an enlarged basis (III) corresponding to 11 harmonic functions and 31 β_s-angle sampling points. The completeness of these bases is assessed in the upper part of Table II by comparing the calculated fundamental frequencies of the water molecule with experimental values.

The lower part of Table II reports the zero-point energy and fundamental intramolecular frequencies at the water dimer equilibrium geometry. The zero-point energies of both monomers, which actually define the ground state adiabatic potential, are practically the same in bases I and II. Basis set I has thus been used for the MW and far IR calculations. Concerning the IR shifts, calculated at the equilibrium geom-

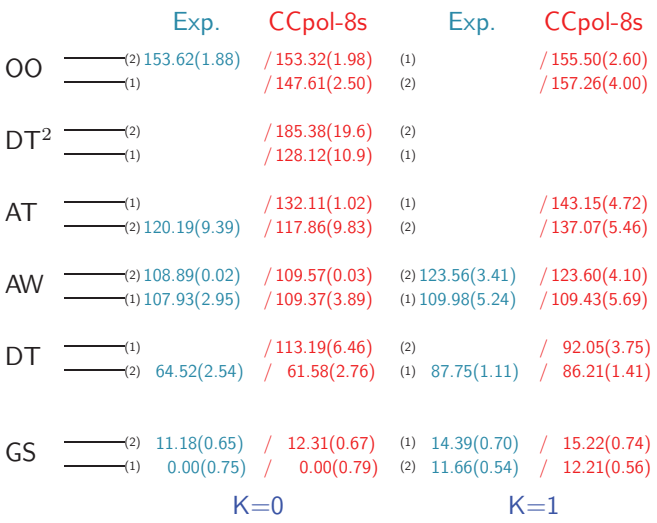

FIG. 2. Experimental[6,8,54,70,71] and calculated (CCpol-8s) VRT levels and tunneling splittings of $(H_2O)_2$: ground state (GS), donor torsion (DT), acceptor wag (AW), acceptor twist (AT), donor torsion overtone (DT^2), and intermolecular stretch (OO). The energies given (in cm^{-1}) correspond to the origins $o_1(K)$ and $o_2(K)$ of the levels (1) and (2) with quantum numbers $K = 0$ and $K = 1$, respectively, as defined in Eq. (39); the values in parentheses are the interchange tunneling splittings $i_1(K)$ and $i_2(K)$, also defined in the text.

etry, one can observe a notable change $\delta(\Delta\omega) = -3.7\,cm^{-1}$ for the O-H_b stretch which constitutes the most anharmonic vibration as it is associated to the hydrogen bond. A further increase in the basis set size (basis III) reveals that no further change appears in the IR shifts, except for a very small one of $-0.5\,cm^{-1}$ for the O-H_b stretch. We thus systematically used basis II for calculating the IR shifts.

2. Intermolecular basis set

Convergence with respect to the intermolecular basis set, explicited in Eq. (37), was assessed by systematically increasing its size. For each intermolecular vibration considered in this work, convergence was tested on both the subfork positions and their associated splittings, as depicted in Fig. 2.

For the $(H_2O)_2$ dimer, we used a Wigner basis up to maximum values of j_A, $j_B = 11$ on the monomers, and a primitive radial basis set of 20 sine functions spanning the range $[4.2 \le \mathcal{R} \le 10]a_0$, contracted to 9 functions by means of the Harris, Engerholm, and Gwinn procedure.[52] A further increase in the Wigner bases, up to $j_A = j_B = 12$, leads to changes less than 0.08 (0.025) cm^{-1} for the subfork positions (splittings). For the ground state results, these values are reduced to 0.06 (0.002) cm^{-1}.

Concerning the $(D_2O)_2$ dimer, a larger intermolecular basis (with maximum $j_A, j_B = 13$ values) had to be used in order to converge the tunneling splittings, which in $(D_2O)_2$ are smaller than in $(H_2O)_2$ by an order of magnitude. Increasing the basis to $j = 14$ changes the excited subfork positions (splittings) by less than 0.14 (0.01) cm^{-1}. These values are reduced to 0.06 (0.001) cm^{-1} for the ground state.

The intramolecular calculations were systematically conducted in the 6D full variational approach, which takes into account the vibrational coupling between monomers and leads to the global [6+6]D formulation. We will, however, mention how the [6+[3+3]]D and [6D+6Dp] approximations compare with it.

B. $(H_2O)_2$ intermolecular VRT levels and splittings

1. Rigid-monomer results

In order to assess the changes due to monomer flexibility, we first show in Fig. 2 the experimental energy levels,[53,54] and those obtained with the rigid version of the CCpol-8s potential.[18] The latter energies were also calculated earlier in Ref. 18 and the two sets are essentially the same. A difference with respect to our previous work is that the energy levels formerly assigned to the donor torsion overtone (DT^2) are reassigned to the O–O stretch. From the associated eigenstates $\psi^{\mathbf{0}}_{\mathbf{n}}(\mathbf{Q})$, we computed the mean radial kinetic energy $\langle\psi^{\mathbf{0}}_{\mathbf{n}}|\hat{T}_{\mathcal{R}}|\psi^{\mathbf{0}}_{\mathbf{n}}\rangle_{\mathbf{Q}}$. For most of the states, this quantity ranges from 30 to 45 cm^{-1}, for both states that we now assign to the O–O stretch the radial kinetic energy is about 80−95 cm^{-1}.

In this diagram, the indices (1) and (2) refer to the $A_1^{\pm}$, $B_1^{\pm}$ and $A_2^{\pm}$, $B_2^{\pm}$ subforks, respectively, that occur for each value of the projection quantum number K. The symbols $A_1^{\pm}$, $B_1^{\pm}$ and $A_2^{\pm}$, $B_2^{\pm}$ refer to the one-dimensional irreps of the molecular symmetry group G_{16} of the water dimer (see Ref. 18 for a detailed description). The splittings between the (1) and (2) levels are due to acceptor tunneling. As the water dimer is a prolate near symmetric top, the origins o_1 and o_2 of the subforks are customarily defined according to the convention

$$E_i(J, K) = o_i(K) + \frac{B + C}{2}[J(J + 1) - K^2], \qquad (39)$$

where J is the total dimer angular momentum quantum number and $E_i(J, K)$ means the average energy of the $A_i^{+/-}$ and $B_i^{+/-}$ levels pertaining to each subfork. The origin $o_1(K = 0)$ is set to zero, so that all other values of $o_i(K)$ should be considered as excitation energies. The values given in parentheses correspond to the splittings $i_i(K) = |A_i^{+/-} - B_i^{+/-}|$ between the levels within each subfork which are due to donor-acceptor interchange tunneling. The acceptor tunneling splitting $a_i(K)$ between the subforks (1) and (2) is defined as $|o_1(K) - o_2(K)|$.

2. Test of some approximations for flexible monomers

We have shown in Sec. III B that, within the adiabatic approximation, one can recast the 12-dimensional calculation for flexible monomers into a series of calculations of the intramolecular vibrations on a grid of intermolecular coordinates $\mathbf{Q}$, which yields a set of adiabatic potentials, and a pseudo-rigid monomer calculation of the intermolecular VRT states on one of these adiabatic potentials. However, the resulting $\mathbf{Q}$-dependence of the monomer rotational constant matrices $\mathbf{\Gamma}$ renders the Lanczos iterative diagonalization scheme about one order of magnitude more costly. The reason is that one has to switch from the spectral to the grid representation many times in order to evaluate the effect of the monomer

rotation operators $\hat{T}_R^X$. The perturbative approach defined by Eqs. (32)−(36) allows one to retrieve the exact transition energies and splittings to within 0.03%. If we ignore the final perturbation step in Eq. (36), the errors increase to about 1%.

The second series of tests concerns the calculation of the adiabatic potential $V_N^{(\mathrm{ad})}(\mathbf{Q})$ as detailed in Sec. III C. We compared the results for the MW and far IR transitions obtained, respectively, in the [6+[3+3]]D approximation, i.e., completely neglecting the six-dimensional $V^{AB}(\mathbf{q}^A, \mathbf{q}^B; \mathbf{Q})$ correction term of Eq. (19), and in the full variational treatment [6+6]D of this term by means of Eq. (24).

We found that, for excited states, the transition energies $o_i(K)$ are lower in the [6+6]D treatment than in the [6+[3+3]]D approximation, but the decrease does not exceed 1 cm^{-1}. The associated interchange splittings $i_i(K)$ differ by 0.5 cm^{-1} at most. For the ground state, these values are 0.25 cm^{-1} and 0.036 cm^{-1}, respectively. The calculations presented in the following were systematically conducted in the full variational [6+6]D treatment. The results corresponding to the [6D + 6Dp] perturbative approach, not shown here, are essentially indistinguishable from those obtained within the [6+6]D variational one.

Finally, we compare the results obtained from either $\mathbf{q}$-averaging the rotational constant matrices $\mathbf{\Gamma}^{X(\mathbf{0})}$ as given by Eq. (29), or using their optimized values $\mathbf{\Gamma}^{X(\mathrm{opt})}$ from Eq. (30). It should be kept in mind that the adiabatic potentials are identical in both cases, only the rotational constant matrices $\mathbf{\Gamma}^X$ differ. For the excited states, the differences in the $o_i(K)$ levels are marginal, between 0 and 0.6 cm^{-1} ($\leq$0.5%), smaller than the deviation from experimental results when available. The corresponding splittings $i_i(K)$ show changes of about 4%, with the exception of the very small acceptor wag $i_2(0)$ value. For the ground state, the changes are about 1% for the energy levels $o_i(K)$. The associated splittings $i_i(K)$ are systematically decreased by 0.02 cm^{-1} when moving from optimized to averaged rotational constants.

In Table III, we show the comparison between optimized $\mathbf{q}_{\mathrm{opt}}$ and vibrationally averaged $\mathbf{q}_{\mathrm{avg}}$ internal monomer coordinates at the water dimer equilibrium geometry $\mathbf{Q}_{\mathrm{eq}}$. Also given are the values $\mathbf{q}_{\mathrm{ref}}$ for the monomer reference geometry obtained by averaging over the isolated monomer ground state vibrational wave functions and used in the rigid CCpol-8s potential. Not surprisingly, the optimized values of r_1 and r_2 are systematically smaller than all the values obtained by vibrational averaging. Among the latter, we observe that the r_1 and r_2 values are larger when averaged over the adiabatic monomer wave functions in the dimer than when averaged over the isolated monomer wave functions. The lower part of the table lists the associated monomer rotational constants $\Gamma_{\alpha\alpha}^X(\mathbf{Q}_{\mathrm{eq}})$. With the exception of Γ_{zz}, the adiabatically averaged constants are closer to the reference values.

TABLE III. Optimized $\mathbf{q}_{\mathrm{opt}}$ [Eq. (18)] and averaged $\mathbf{q}_{\mathrm{avg}}$ [Eq. (29)] internal coordinates (r_1, r_2, β) (in a_0 and radians) of the acceptor (A) and donor (D) moieties at the water dimer equilibrium geometry; $\mathbf{q}_{\mathrm{ref}}$ refers to the fixed (isolated monomer averaged) values used in the rigid CCpol-8s potential. The lower part of the table reports the corresponding ground-state rotational constants $\Gamma_{\alpha\alpha}^X$ in cm^{-1}. The constants in the last column are those denoted as $\Gamma_{\alpha,\alpha}^{X(0)}$ in the text.

$\mathbf{q}$	$\mathbf{q}_{\mathrm{ref}}$	$\mathbf{q}_{\mathrm{opt}}$	$\mathbf{q}_{\mathrm{avg}}$
r_1^A	1.836	1.812	1.845
r_2^A	1.836	1.812	1.845
θ^A	1.827	1.827	1.827
r_1^D	1.836	1.818	1.855
r_2^D	1.836	1.809	1.841
θ^D	1.827	1.827	1.828
Γ_{xx}^A	9.2778	9.4914	9.2937
Γ_{yy}^A	27.8806	27.4240	28.0047
Γ_{zz}^A	14.5216	14.5151	14.4274
Γ_{xx}^D	9.2778	9.4775	9.2646
Γ_{yy}^D	27.8806	27.4055	27.9094
Γ_{zz}^D	14.5216	14.4872	14.3773

3. Flexible-monomer results

In Fig. 3, we report the energy levels, i.e., the origins $o_1(K)$ and $o_2(K)$ for $K = 0$ and $K = 1$, and the interchange tunneling splittings $i_1(K)$ and $i_2(K)$ calculated with the full flexible potential in the [6+6]D adiabatic approximation. Also the available experimental data are included in this figure. When comparing this figure with Fig. 2, we can observe the effects of using flexible monomers, rather than rigid ones. The agreement with the experimental data, which was already very good for the rigid CCpol-8s potential, remains about equally good for the flexible-monomer potential CCpol-8s*f*. Only for the O–O stretch mode, the result slightly deteriorates by including monomer flexibility: the frequency obtained from CCpol-8s*f* is lower than the experimental value by about 4 cm^{-1}, while the frequency obtained from CCpol-8s agreed to 0.3 cm^{-1}. This might be related to the fact that, as shown in Table I, the SAPT-5s′*f*IR hydrogen bond length (O_a-H_b) is too large by about 0.06 Å as compared to the benchmark calculations of Tschumper *et al.*[30] Although the O_a-H_b hydrogen bond length from the CCpol-8s*f* potential agrees much better with the corresponding result of Tschumper *et al.*,

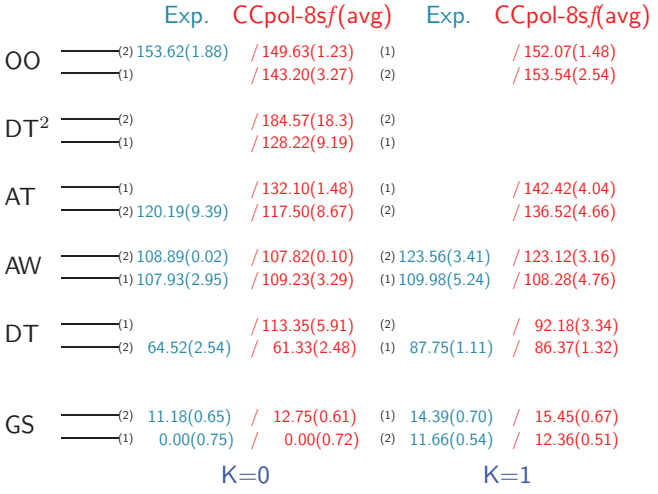

FIG. 3. Comparison of experimental VRT levels and tunneling splittings with results calculated with the CCpol-8s*f* potential using averaged values of the $\mathbf{\Gamma}^X$ rotational matrices. For definitions, see Fig. 2.

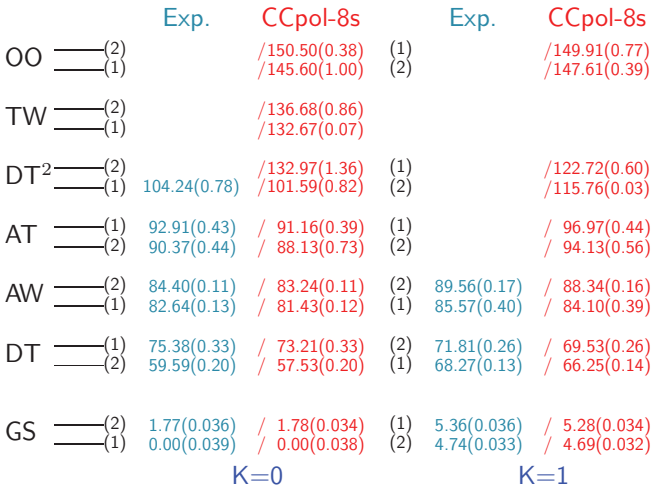

FIG. 4. Comparison of $(D_2O)_2$ experimental VRT levels and tunneling splittings with values obtained from the rigid CCpol-8s potential. For definitions, see Fig. 2. The symbol TW stands for a combination of the donor torsion and acceptor wag mode.

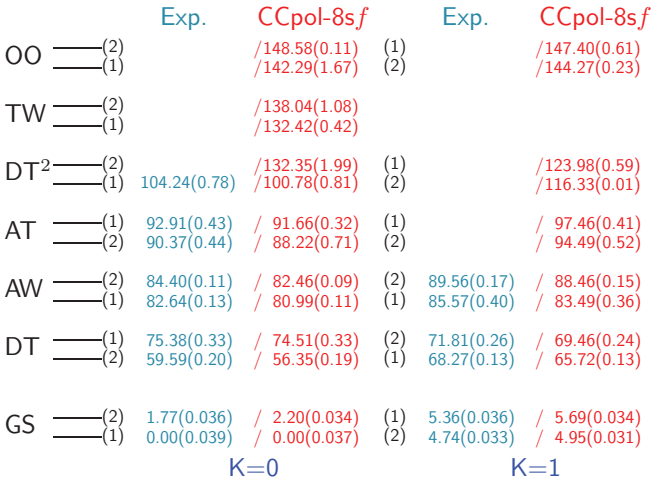

FIG. 5. Comparison of $(D_2O)_2$ experimental VRT levels and tunneling splittings with values obtained from the flexible-monomer CCpol-8s*f* potential. For definitions, see Figs. 2 and 4.

the hydrogen bond (or O–O) stretch motion might be less well described by the monomer flexibility correction in CCpol-8s*f*, which was taken from SAPT-5s′*f*IR, cf. Eq. (6). The O–O stretch frequency difference of 4 cm^{-1} amounts to a relative error of only 2.7%, however, so this deviation may also be accidental.

As a final test, we compare the dissociation energy $D_0 = 1108.2\ cm^{-1}$ obtained from the CCpol-8s*f* potential with the experimental value $1105 \pm 10\ cm^{-1}$ recently measured by Rocher-Casterline and co-workers[55] by velocity map imaging. The calculated value is off by only 3 cm^{-1}, well within the experimental error bars, which tends to validate both this new potential and the method used to perform the VRT level calculations. It should be noted that the rigid-monomer CCpol-8s potential leads to a dissociation energy $D_0 = 1094\ cm^{-1}$, demonstrating the need for a flexible-monomer description in order to precisely reproduce some of the properties of the dimer.

C. Intermolecular VRT levels for $(D_2O)_2$

We first present in Fig. 4 the results obtained from the rigid-monomer CCpol-8s potential. These calculations were conducted with a larger intermolecular basis (with maximum $j_A, j_B = 13$) as mentioned previously. Convergence tests, described in Sec. IV A 2, show that further changes with respect to the basis set size are smaller than the deviations from the available experimental results. The results differ slightly from the corresponding results in Ref. 18, because the basis in that study was smaller. The O–O stretch levels were assigned on the basis of a considerably higher radial kinetic energy, just as the corresponding levels in $(H_2O)_2$.

For the flexible-monomer calculations, we first compared the averaged and optimized $\mathbf{\Gamma}$ matrices using the same, $j_A, j_B \leq 13$, intermolecular basis in the [6+[3+3]]D approximation. It was found that the energies $o_i(K)$ changed by 0.036 at most ($\leq$1.6%) and by $0.30\ cm^{-1}$ ($\leq$0.4%) for the ground and excited states, respectively. For the interchange tunneling splittings $i_i(K)$, these values are reduced to 0.001 and $0.018\ cm^{-1}$, respectively (that is, 2%−3%). All these differences are considerably smaller than the corresponding deviations from the available experimental results. Hence, the effect of using averaged or optimized $\mathbf{\Gamma}$ matrices becomes much less important upon deuteration, which is due to the more localized nature of the intramolecular wave function for the deuterated species.

The larger intermolecular basis set used renders the adiabatic potential calculation step much costlier, as the associated intermolecular coordinate grid has to be larger; it spans 2×10^6 non-symmetry-equivalent points at which the intramolecular eigenvalue problem has to be solved. Hence, we checked that for a smaller, $j_A, j_B \leq 11$, basis perturbative [6D+6D*p*] and full variational [6+6]D calculations gave nearly identical results. For the ground state, the energies $o_i(K)$ changed by $10^{-3}\ cm^{-1}$ at most, while the interchange tunneling splittings $i_i(K)$ varied by less than $10^{-3}\ cm^{-1}$. For excited states, these changes corresponded to 10^{-2} at most and $10^{-3}\ cm^{-1}$, respectively. In all cases, these variations are well below the intrinsic convergence limit for the intermolecular basis with $j_A, j_B \leq 13$ retained for the calculations. The flexible-monomer calculations presented in Fig. 5 were thus performed with the $j_A, j_B \leq 13$ basis within the perturbative [6D+6D*p*] treatment, using averaged $\mathbf{\Gamma}$ matrices.

The inclusion of the correlation $V^{AB}(\mathbf{q}^A, \mathbf{q}^B; \mathbf{Q})$ between the intramolecular vibrations, Eq. (19), by perturbation theory, cf. Eq. (23), essentially left the ground state characteristics unchanged, while the energies of the excited states changed at most by a few times 0.1 cm^{-1} and the splittings by a few times 0.01 cm^{-1}. Again, this effect can be understood from the increased localization of the intramolecular wave functions of D_2O, relative to H_2O.

Figure 5 presents a comparison of the VRT levels and splittings calculated on the flexible-monomer CCpol-8s*f* potential with the experimental data.[8,53,54,56–58] No significant differences are observed with respect to the rigid CCpol-8s results in Fig. 4, the good agreement with the available experimental data remains.

TABLE IV. Frequency shifts of the monomer vibrations (in cm^{-1}) in the water dimer. For definitions, see Table II. The G_{16} and G_8 models are defined in the text. Except for the rightmost column obtained with optimized values of the $\mathbf{\Gamma}$ matrices, the calculations were performed with the averaged ones.

	[6+6]D	[6+[3+3]]D		
Intramolecular mode	G_{16}	G_{16}	G_8	G_{16}[opt]
$b[D]$	+13.4	+13.7	+14.8	+9.1
O–$H_b[D]$	−61.6	−57.9	−59.0	−55.1
O–$H_f[D]$	−13.5	−17.6	−18.9	−14.7
$b[A]$	+7.3	+9.6	+7.5	+4.4
$ss[A]$	−7.1	−8.6	−8.7	−6.2
$as[A]$	−6.6	−10.4	−9.0	−7.2

D. Frequency shifts of the monomer modes in $(H_2O)_2$

In Sec. III D we explained that, in contrast to the ground state, the adiabatic [6+6]D approximation is not completely valid if one of the monomers is vibrationally excited. We proposed two approximate adiabatic models, called G_{16} and G_8, that should give a good approximation to the more rigorous "two-state" non-adiabatic model that is appropriate for the vibrationally excited states. It may be expected that a comparison of the results of the G_{16} and G_8 models for the vibrational frequency shifts will give us a good indication of the accuracy of the shifts calculated by either model.

The frequency shift of each monomer vibration was obtained by subtracting the energy of the dimer ground state level computed on the lowest adiabatic 6D potential (with both monomers in their ground state) from the dimer ground state level computed on the excited adiabatic potential obtained for the corresponding monomer vibration. In the G_8 model, one can choose which monomer is excited, A or B; the results are the same. Since a given monomer excited state gives rise to two dimer excitations in the G_8 model, one on the donor and one on the acceptor, we had to consider the lowest two eigenvalues from each calculation. The acceptor can be identified *a posteriori* as the monomer that has its O atom in the shortest hydrogen bond $O_a \cdots H_b$. A comparison of the results from the G_{16} and G_8 models is given in Table IV. Furthermore, we show in this table what is the effect of simplifying the full adiabatic [6+6]D approach to the computationally cheaper [6+[3+3]]D approximation, as well as the effect of taking monomer rotational constant matrices Γ^X calculated at the optimized monomer geometries, instead of using the values averaged over the adiabatic monomer wave functions.

Before discussing the results, we must also explain the symmetry of the intramolecular vibrations and the appropriate selection rules. The water dimer in its equilibrium geometry has a mirror plane, point group C_s. The donor monomer (D) lies in the plane of reflection and its symmetric and asymmetric OH stretch modes become localized. One of them is the O–H stretch mode of the H atom involved in the hydrogen bond, O–H_b, the other one is the O–H stretch mode of the free H atom, O–H_f. Both modes have A' symmetry in C_s. The two H atoms of the acceptor monomer (A) stick out of the symmetry plane; they are interchanged by the reflection symmetry operator. The acceptor symmetric O–H stretch (*ss*) mode has A' and the asymmetric O–H stretch (*as*) mode has A'' symmetry. The HOH bend modes of both monomers have A' symmetry. Since the water dimer tunnels between eight equivalent equilibrium geometries of this type, we must use the molecular symmetry group G_{16}, instead of the point group C_s. The intramolecular vibrations are all of A_1^+ symmetry, except for the $as[A]$ mode which is of A_2^+ symmetry. Actually, if the $as[A]$ mode were adapted to the full G_{16} symmetry, one would obtain A_2^+ and B_2^+ symmetry components, but we already explained above that the adiabatic separation of the monomer vibrational coordinates and the intermolecular coordinates does not fully apply to the excited intramolecular vibrations. Hence, it is reasonable to apply the selection rules of the subgroup G_8, as it was done in the interpretation of the high-resolution spectra in Ref. 5. In G_8 symmetry, the G_{16} irreps A_2^+ and B_2^+ become equivalent. If one (or more) of the intermolecular (tunneling or vibrational) modes is excited, their symmetries should be combined with those of the intramolecular modes, as well as with those of the overall rotation functions of the dimer. The transition dipole moment operator has A_1^- symmetry, which tells us that transitions are allowed between irreps of the same type, except for the ± labels which must be reversed. This is a strict selection rule. In addition, there are approximate selection rules based on the separability between the intra- and intermolecular vibrations. Furthermore, there may be approximate selection rules if the vibrations have small amplitudes and can be well separated from the overall rotations. This does not apply to the intermolecular vibrations,[59] but it holds for the intramolecular modes which obey the selection rules of the point group C_s.

All fundamental intramolecular modes are allowed in the water dimer, as they are in the free monomers. For all modes except $as[A]$, we report in Table IV the shifts associated with the $A_1^-[J'=1, K'=0] \leftarrow A_1^+[J''=0, K''=0]$ transitions belonging to the lower acceptor tunneling components. These transitions may be considered as pure intramolecular vibrational fundamentals, accompanied only by a change $\Delta J = 1$ in total angular momentum that does not alter the internal motions in the dimer. For the $as[A]$ mode, such transitions are forbidden; the excitation of this mode is only allowed in combination with a change in the projection quantum number K. As one can see in Figs. 2 and 3, the VRT levels for $K = 0$ are quite different from the levels for $K = 1$, so it is clear that the change of K affects the internal motions of the monomers in the dimer. In Table IV, we report the allowed $A_1^+[J'=1, K'=1] \leftarrow A_2^-[J''=0, K''=0]$ transition for the $as[A]$ mode, which was also measured.[5]

Within the [6+[3+3]]D approximation (rightmost columns in the table), we first assessed the changes in the frequency shifts upon using averaged or optimized $\mathbf{\Gamma}$ matrices in the G_{16} model. It can be seen that the shifts are considerably modified, in some cases by as much as 5 cm^{-1}. The explanation of these relatively large differences is that these shifts result from transitions to excited adiabatic potentials which correspond to more delocalized intramolecular wave functions than the ground state. Therefore, the averaging can substantially modify the $\mathbf{\Gamma}$ matrices and we used it in all

TABLE V. Calculated frequency shifts of the monomer vibrations in $(H_2O)_2$ for $J = 0 \rightarrow 1$ and $J = 1 \rightarrow 0$ dimer transitions. The symmetries indicated refer to the intermolecular VRT levels that produce allowed transitions in combination with the intramolecular mode. For the $K = 1 \rightarrow 0$ transitions in the last column, the symmetries of the initial and final states are reversed.

	Transition	Frequency shift (cm^{-1})		
Intramolecular mode	Symmetry	$K = 0 \rightarrow 0$	$K = 0 \rightarrow 1$	$K = 1 \rightarrow 0$
$b[D]$	$A_1^+ \rightarrow A_1^-$	13.39	29.60	–4.22
	$B_1^+ \rightarrow B_1^-$	11.84	28.12	–2.72
	$A_2^- \rightarrow A_2^+$	14.45	12.81	12.94
	$B_2^- \rightarrow B_2^+$	13.13	11.62	14.16
O–H_b[D]	$A_1^+ \rightarrow A_1^-$	–61.63	–47.17	–78.89
	$B_1^+ \rightarrow B_1^-$	–62.83	–48.33	–77.75
	$A_2^- \rightarrow A_2^+$	–63.15	–62.96	–64.37
	$B_2^- \rightarrow B_2^+$	–64.17	–63.91	–63.45
O–H_f[D]	$A_1^+ \rightarrow A_1^-$	–13.47	1.20	–30.91
	$B_1^+ \rightarrow B_1^-$	–14.85	–0.13	–29.58
	$A_2^- \rightarrow A_2^+$	–14.42	–14.42	–15.81
	$B_2^- \rightarrow B_2^+$	–15.61	–15.52	–14.72
$b[A]$	$A_1^+ \rightarrow A_1^-$	7.26	22.84	–10.37
	$B_1^+ \rightarrow B_1^-$	5.68	21.34	–8.85
	$A_2^- \rightarrow A_2^+$	7.55	6.60	6.07
	$B_2^- \rightarrow B_2^+$	6.26	5.40	7.26
$ss[A]$	$A_1^+ \rightarrow A_1^-$	–7.06	7.84	–24.64
	$B_1^+ \rightarrow B_1^-$	–8.59	6.38	–23.17
	$A_2^- \rightarrow A_2^+$	–7.49	–7.94	–8.95
	$B_2^- \rightarrow B_2^+$	–8.76	–9.12	–7.79
$as[A]$	$A_1^+ \rightarrow A_2^-$		3.48	–21.57
	$B_1^+ \rightarrow B_2^-$		3.22	–21.43
	$A_2^- \rightarrow A_1^+$		–6.65	–12.73
	$B_2^- \rightarrow B_1^+$		–6.65	–12.82

subsequent calculations. We then considered the two limiting models, G_{16} and G_8. The results from these two models are quite similar, the largest difference being about 2 cm^{-1}. The smallest difference one might expect is about half of the size of the ground state interchange tunneling splitting $i_1(K)$, cf. Fig. 3, since this splitting is given by the G_{16} calculations but not by the G_8 model.

The first column in Table IV provides the calculated shifts obtained within the [6+6]D full variational approach, using averaged $\mathbf{\Gamma}$ matrices. Comparison with the second column allowed us to estimate the importance of the residual coupling term $V^{AB}(\mathbf{q}^A, \mathbf{q}^B; \mathbf{Q})$ between the two monomers, cf. Eq. (19). This coupling is particularly important for the donor O–H stretches and the acceptor asymmetric stretch modes, resulting in changes as large as 4 cm^{-1}. In all further calculations, we used the full [6+6]D adiabatic approach and the G_{16} model.

The frequency shifts of the allowed $J = 0 \rightarrow 1$ and $J = 1 \rightarrow 0$ transitions are listed in Table V for all six fundamental intramolecular modes. It is assumed that only different intermolecular tunneling components of the ground and excited states take part in these transition, and that the intermolecular vibrations are not excited. It should be kept in mind that for $(H_2O)_2$ the $A_1^\pm$, $B_1^\pm$, $A_2^\pm$, and $B_2^\pm$ levels have nuclear spin statistical weights 1, 0, 3, and 6, respectively. In addition, there are transitions between the levels of $E^\pm$ symmetry with weight 3 which are not shown; their shifts are intermediate between those involving the $A_1^\pm$, $A_2^\pm$ and $B_1^\pm$, $B_2^\pm$ levels. As it was already mentioned above, the interchange splittings between the $A_1^\pm$ and $B_1^\pm$ components and between the $A_2^\mp$ and $B_2^\mp$ components are exaggerated in our G_{16} model calculations, because the excited state interchange splittings are actually much smaller. The energy gaps between the A_1^+, B_1^+ levels and the A_2^-, B_2^- levels, caused by acceptor tunneling, are much larger. These gaps are not reflected in the frequency shifts of the $K = 0 \rightarrow 0$ transitions because these transitions occur from the lower to the lower or from the upper to the upper acceptor tunneling levels. Such $K = 0 \rightarrow 0$ transitions are not allowed for the acceptor asymmetric stretch mode, due to the A_2^+ symmetry of this mode. The acceptor tunneling splitting is considerably smaller for $K = 1$ than for $K = 0$ and the order of the tunneling levels is reversed, hence, the $K = 0 \rightarrow 1$ and $K = 1 \rightarrow 0$ transitions have rather different frequency shifts for transitions involving the A_1^+, B_1^+ levels or the A_2^-, B_2^- levels.

Although experimental data from IR spectroscopy are available for each of the $(H_2O)_2$ monomer modes, it is not straightforward to compare our calculated frequency shifts with these data. The measured frequency shifts originate from very different sources: high-resolution molecular beam IR spectra[5,20] only for the $as[A]$ mode, cavity ringdown spectra[60] for the bend modes, size-selected cluster molecular beam spectra,[61,62] matrix spectra in solid noble gas matrices,[21,63] and matrix spectra in very cold helium droplets[9] for all the O–H stretch modes. In the lower resolution spectra, the bands are quite broad and not resolved, so it is not clear which of the calculated tunneling components and rotational transitions actually correspond to the frequency shifts extracted from these spectra. In matrix spectra, the frequencies are shifted by an unknown amount due to the effect of the surrounding matrix, although such shifts are probably small in the case of helium droplets. In Table VI, we summarize the experimental data and compare them with the calculated results with which they should most probably be associated.

The most detailed and best defined information is available for the acceptor asymmetric stretch mode. In the high-resolution spectrum of this mode measured by Huang and Miller,[5] they observed three different bands corresponding to the $K = 1 \rightarrow 0$, $K = 0 \rightarrow 1$, and $K = 1 \rightarrow 2$ transitions; many rotational lines in these bands were assigned and fitted. The frequencies obtained for the $K = 1 \rightarrow 0$ and $K = 0 \rightarrow 1$ transitions of $A_2^- \rightarrow A_2^+$ symmetry are 3738.4 and 3752.6 cm^{-1}, respectively, which corresponds to shifts of –17.4 and –3.2 cm^{-1} relative to the H_2O monomer asymmetric stretch frequency. The same mode was observed by Kuyanov, Choi, and Vilesov[9] for the water dimer in helium nanodroplets in a molecular beam setup. These authors reported two peaks with frequency shifts of –3.4 and 4.4 cm^{-1}. One of the peaks may correspond to the same $K = 0 \rightarrow 1$ transition observed by Huang and Miller, but the other peak is not the $K = 1 \rightarrow 0$ transition, since the energy gap between the two peaks is smaller by nearly a factor of two than the energy difference between the $K = 0 \rightarrow 1$ and $K = 1 \rightarrow 0$ transitions in Ref. 5 and it is believed that the $K = 1$ levels are not populated at the temperature of 0.4 K of the He droplets. Our calculations show that the two peaks in the spectrum of Ref. 9 are

TABLE VI. Measured frequency shifts of the monomer vibrations (in cm^{-1}) in $(H_2O)_2$ and the corresponding calculated values from different potentials, see text. The calculations with the CCpol-8s*f* potential used the adiabatic G_{16} full [6+6]D model with averaged **Γ**. The values given are averages of values from Table V, as specified in the last column. For definitions, see Table II.

Intramolecular		Calculated				
mode	Expt.	CCpol-8s*f*	SAPT-5s′*f*IR[a]	HBB[b]	HBB2[c]	Specification[d]
b[*D*]	+20[e]	+13.2	+5	+9.6	+16.3	$K=0\rightarrow 0$
O–H$_b$[*D*]	−56,[f] −59.0[g]	− 62.9	−52	− 42.5	− 46.3	$K=0\rightarrow 0$
O–H$_f$[*D*]	−21,[f] −25.3 and −26.3[g]	− 14.6	−15	− 2.1	− 23.5	$K=0\rightarrow 0$
b[*A*]	+6[e]	+6.7	+4	+2.8	+6.9	$K=0\rightarrow 0$
ss[*A*]	−2.2[g] (−2 to +3[h])	− 8.0	−7	− 0.4	− 3.0	$K=0\rightarrow 0$
as[*A*]	−17.4[i]	− 21.5		− 5.5	− 20.8	$K=1\rightarrow 0$[j]
	−3.4,[g] −3.2[i]	− 6.6	−12	+9.8	− 5.9	$K=0\rightarrow 1$[k]
	+4.4[g]	+3.4		+18.5	+3.1	$K=0\rightarrow 1$[l]

[a]Calculated in Ref. 25.
[b]Calculated in Ref. 34.
[c]Calculated in Ref. 64.
[d]The $K=0\rightarrow 0$ transition frequencies differ only slightly for different irreps, see Table V; we averaged over all symmetry components.
[e]From cavity ringdown spectra (Ref. 60).
[f]From size-selected cluster molecular beam spectra (Refs. 61 and 62).
[g]From helium droplet spectra (Ref. 9).
[h]Extrapolated value from solid noble gas matrix spectra (Refs. 21 and 63).
[i]From molecular beam high-resolution spectra (Refs. 20 and 5).
[j]$A_2^-/B_2^- \rightarrow A_1^+/B_1^+$.
[k]$A_2^-/B_2^- \rightarrow A_1^+/B_1^+$.
[l]$A_1^+/B_1^+ \rightarrow A_2^-/B_2^-$.

probably due to the A_2^-, B_2^- and A_1^+, B_1^+ tunneling components of the $K=0\rightarrow 1$ transition.

The frequency of the acceptor symmetric stretch mode was determined in matrix spectra.[21,63] Extrapolation of the spectra from different matrices yields a frequency between 3655 and 3660 cm^{-1}, i.e., a shift between –2 and 3 cm^{-1}. In the helium nanodroplet spectra,[9] this band was observed at 3654.4 cm^{-1}, which amounts to a shift of –2.2 cm^{-1}.

The donor bound and free OH stretch modes were observed in lower resolution by Huisken *et al.*[61,62] A narrow peak at 3601 cm^{-1}, shifted by –56 cm^{-1} with respect to the monomer symmetric stretch mode, was assigned to the bound OH stretch. Apart from the reassignment, this agrees well with the (incomplete) high-resolution data for this band in Ref. 5. Absorption intensity at 3735 cm^{-1}, obtained by subtraction of two spectra, was ascribed to the donor free OH stretch; this amounts to a shift of –21 cm^{-1} with respect to the monomer asymmetric stretch mode. The He droplet spectra of the water dimer[9] give a shift of –59.0 cm^{-1} for the donor bound OH stretch mode and two, not completely separated peaks with shifts of –25.3 and –26.3 cm^{-1} for the donor free OH stretch.

Some additional remarks can be made regarding the He nanodroplet spectra,[9] which show bands for all four OH stretch modes. Only for the acceptor asymmetric stretch mode a large splitting (7.8 cm^{-1}) was measured, while for the other modes only a small splitting (1.0 cm^{-1} for the donor free OH stretch) or no splitting was observed. A similar splitting of the acceptor asymmetric stretch band was measured and explained by interchange tunneling[58] for $(D_2O)_2$. It should be kept in mind that the acceptor asymmetric stretch mode is the only one for which $K=0\rightarrow 0$ transitions are forbidden. As explained above, we believe that the peaks in the He droplet spectra assigned to the acceptor asymmetric stretch mode belong to a $K=0\rightarrow 1$ band; our calculations predict an acceptor tunneling splitting of the correct size for this band. As also explained above, we predict much smaller tunneling splittings for $K=0\rightarrow 0$ transitions. This implies that the absorption intensities of all bands in the He droplet spectra, except for the acceptor asymmetric stretch band, are probably dominated by $K=0\rightarrow 0$ transitions.

The donor and acceptor bend modes were observed by Paul *et al.* in cavity ringdown spectra.[60] A peak at 1600.6 cm^{-1}, i.e, a blueshift of 6 cm^{-1}, was assigned to the acceptor bend, probably involving a parallel $\Delta K=0$ transition. From three peaks at 1613.8, 1614.7, and 1628.6 cm^{-1} in the spectrum,[60] it was estimated that the donor bend frequency is 1615–1620 cm^{-1}, a blueshift of more than 20 cm^{-1} with respect to the monomer bend. According to Ref. 60, these bands are dominated by perpendicular $\Delta K=\pm 1$ transitions. Our shifts calculated for $K=0\rightarrow 0$ transitions in the donor bend mode are about +13 cm^{-1}, for the $K=0\rightarrow 1$ and $K=1\rightarrow 0$ transitions they vary from –4 to +30 cm^{-1}. It is not clear which components dominate the intensities of these bands, but we included the value calculated for the $K=0\rightarrow 0$ transition in Table VI.

For all transitions, except for the acceptor asymmetric stretch mode, we included in Table VI the averages of the calculated transition frequencies listed in Table V for the $K=0\rightarrow 0$ transitions. The results computed with the HBB and HBB2 potentials in Refs. 34 and 64 were treated similarly. Our reason for doing this is that the transition frequencies of the different symmetry components are quite similar for $\Delta K=0$ transitions, so we expect that in the (lower resolution) spectra the absorption bands are dominated by such transitions. Table VI shows that the IR frequency shifts calculated in the [6+6]D model with the CCpol-8s*f* potential agree quite well with the available experimental data, better than

TABLE VII. Frequency shifts of the intramolecular modes in $(H_2O)_2$ calculated in the harmonic approximation (in cm^{-1}). For experimental values, see Table VI.

Mode	CCpol-8s*f*	SAPT-5s′*f*IR[a]	Tschumper *et al.*[30]
$b[D]$	+18.8	+17.5	+26.7
O–$H_b[D]$	− 48.3	− 43.5	− 82.7
O–$H_f[D]$	− 26.8	− 24.1	− 29.0
$b[A]$	+4.2	+3.1	+1.8
$ss[A]$	− 3.5	− 6.1	− 5.7
$as[A]$[b]	− 9.3	− 10.0	− 9.7

[a]The reason why these values differ from those in Ref. 25 is explained in the text.
[b]Since the harmonic approximation cannot distinguish between tunneling levels, its prediction for the $as[A]$ shift is usually compared with the experimental value of $-11\ cm^{-1}$ from Table V in Ref. 5.

the results obtained with the SAPT-5s′*f*IR potential[25] and the HBB potential,[34] although the improvement over the SAPT-5s′*f*IR results is small except for the $b[D]$ mode. This holds also for the acceptor asymmetric stretch mode, where experimental data are available for the individual symmetry components, both for $K = 0 \rightarrow 1$ and $K = 1 \rightarrow 0$ transitions. The agreement with experiment achieved by the HBB2 potential is generally comparable to that of CCpol-8s*f*. The former shifts are somewhat better for the donor bend, free O–H stretch, and acceptor symmetric stretch modes, but the latter potential provides a much better agreement with experiment for the most significantly shifted donor bound O–H stretch mode.

As discussed earlier, the harmonic approximation works relatively well for the IR frequency shifts of the intramolecular modes, so we also computed harmonic frequencies for both the CCpol-8s*f* and SAPT-5s′*f*IR potentials. The force constants are the second derivatives of the potential with respect to the same intra- and intermolecular coordinates as used in the calculations of the VRT levels, computed at the dimer equilibrium geometry. The frequencies calculated with the SAPT-5s′*f*IR potential differ slightly from those in Ref. 25, since we discovered that the original SAPT-5s′*f*IR potential had an error in one of the expansions in monomer coordinates that violated the permutational symmetry. We restored the symmetry in the potential, but since the optimizations of the potential parameters were performed with the error, the parameters were not completely optimal. Very recently, we repeated the optimization with the correct symmetry[65] and the resulting potential is very close to the original one. The effect of this symmetrization on the spectra is very small: most of the IR shifts change by less than $1\ cm^{-1}$, the largest change is $3\ cm^{-1}$ for the O–$H_b[D]$ mode. The results for the intramolecular modes, listed in Table VII, can be compared with the best harmonic frequencies in the literature computed directly at CCSD(T) level in an augmented basis set of between double- and triple-zeta quality by Tschumper *et al.*[30] Note that in Ref. 30 the energies of the characteristic points are highly converged benchmark values, but the harmonic frequencies can probably be appreciably improved by using larger basis sets. Table VII shows that the shifts from the two potentials are similar and that the agreement with the results in Ref. 30 is fairly good, except for the large frequency shift of the O–$H_b[D]$ mode. Also the agreement of the results in Ref. 30 with the measured frequency shifts is worst for this mode. For all other modes, the harmonic shifts, both from Ref. 30 and computed by us, agree quite well with the experimental values. For the intermolecular modes and tunneling splittings the harmonic model is completely inappropriate.

V. DISCUSSION

CCpol-8s*f*, the new flexible-monomer *ab initio* water dimer potential presented here, constitutes a definite improvement over the previous SAPT-5s′*f*IR potential.[25] In particular, it has the depth at the minimum $D_e = 21.0\ kJ\ mol^{-1}$ identical to the number of digits given with an accurate benchmark value. As the one-body $V^{(1)}$ term is taken as the spectroscopically accurate PJT2 water potential of Polansky and co-workers,[36] it enforces the correct asymptotic monomer properties.

Calculation of the spectroscopic properties of a non-rigid water dimer constitutes a formidable task, as it formally corresponds to a 12-dimensional problem. To describe the vibrating water monomers, we started from the general cluster formulation of Gatti and Iung[37] which expresses the KEO in a rigorous, compact form and offers the user a choice of internal coordinates. Due to the light-heavy-light nature of the H_2O monomers, Radau vectors constitute an optimal choice and lead to a compact expression of their KEO.

The large frequency separation between inter- and intramolecular modes allowed us to resort to an adiabatic decoupling, and to recast the flexible-monomer calculations of the dimer VRT states into pseudo-rigid ones performed on adiabatic potentials. These potentials are obtained by solving the six-dimensional intramolecular subsystem eigenvalue problem at fixed intermolecular geometries, and assigning the resulting energies of the vibrational manifold. The pseudo-spectral method used to perform pseudo-rigid dimer VRT calculations renders this adiabatic implementation particularly efficient, as the potential is expressed on the six-dimensional intermolecular grid.

Calculations relying on the exact solution of the intramolecular subsystem problem, termed [6+6]D, required a large amount of central processing unit time (up to 40 days on a 12-core computer): in fact, one has to solve a six-dimensional vibrational problem at each point of a six-dimensional grid. Therefore, we also investigated the [6+[3+3]]D approximation which solves the vibrational manifold of each monomer with the other one fixed at its local equilibrium geometry. Even for the accurate CCpol-8s*f* potential used here, the errors resulting from such an approximation represent only a fraction of the deviation from the experimental data. They are, however, more pronounced when considering the frequency shifts of the monomer vibrations observed in IR spectra. This might have been expected since the potential coupling between excited monomers is larger than for ground state monomers.

The intermolecular VRT levels of both $(H_2O)_2$ and $(D_2O)_2$ calculated with the rigid-monomer CCpol-8s potential agree extremely well with the measured high-resolution spectra.[6,18,53] The present calculations show that the flexible-monomer correction which we introduced in the CCpol-8s*f*

potential did not further improve the agreement with experiment for the intermolecular VRT levels; it remains about equally good. Essentially the same conclusion was reached[34] in calculations with the flexible-monomer HBB potential of Bowman and co-workers:[26] when the VRT levels were computed from this potential in [6+6]D calculations with flexible monomers, some of the levels agree slightly better with the experimental data than in 6D calculations with rigid monomers, for other levels the agreement became slightly worse. Only the ground state acceptor tunneling splitting was systematically improved for the HBB potential when the monomers were kept flexible. The present results computed with the CCpol-8s*f* potential may also be compared with similar results obtained recently[64] with the newer HBB2 version[66,67] of the HBB potential. The flexible-monomer HBB2 potential produces slightly better agreement with experiment for the acceptor tunneling splitting in the ground state of the dimer, but for the excited states and for the ground state interchange tunneling splittings the CCpol-8s*f* results are slightly superior. Disregarding these subtle differences, it may be stated that the potentials discussed above produced VRT levels that agree very well with the MW and far IR data. Earlier calculations of the VRT levels of $(H_2O)_2$ and $(D_2O)_2$ with the various available water potentials have shown, however, that this is certainly not the case for all water potentials. In fact, in addition to the SAPT, CCpol, and HBB potentials, only the empirical VRT(ASP) potentials fitted to dimer spectra are in same league in terms of agreement with experiment. It may be reiterated that the comparison of accurately calculated VRT levels of the water dimer with high-resolution experimental data constitutes a very critical test of the quality of the intermolecular potential, a test that is failed by most of the available water potentials.

Table VI shows that the frequency shifts of the monomer vibrations obtained with the CCpol-8s*f* potential constitute a definite improvement when compared to the results in Ref. 34 computed with the HBB potential. They are also slightly better than the shifts obtained[25] from the SAPT-5s′*f*IR potential. The frequency shifts obtained in Ref. 64 with the HBB2 potential agree about equally well with experiment as the shifts obtained here with the CCpol-8s*f* potential. The shifts from the HBB2 potential are somewhat better for the donor bend, free O–H stretch, and acceptor symmetric stretch modes, the CCpol-8s*f* potential produces a much better shift for the donor bound O–H stretch mode.

Three possible explanations can be given for the remaining discrepancies between theory and experiment:

1. Most of the intramolecular modes (an exception is the acceptor asymmetric stretch mode) were only observed in lower resolution molecular beam spectra with rather broad bands, in which the fine structure due to rotations and tunneling was not resolved, or in matrix spectra. The experimental frequencies extracted from these spectra mostly correspond to some maximum in the absorption bands, sometimes after subtraction of other bands. Therefore, it is uncertain what these frequencies actually correspond to, and to which of the calculated transition frequencies they should be compared.
2. The accuracy of the [6+6]D adiabatic model used for the water dimer with flexible monomers has not yet been evaluated. This is particularly relevant for the excited intramolecular vibrations since, as explained above, a formally correct treatment of the monomer excited states would require a "two-state" non-adiabatic model. The shifts computed by the more approximate adiabatic models, called G_{16} and G_8, may be amenable to improvement.
3. One can estimate[68] that residual inaccuracies of potential surfaces due to post-CCSD(T) excitations, basis set truncations, and fit imperfections are of the order of 1% of interaction energy, i.e., about 20 cm^{-1} in the minimum region. This value is larger than most discrepancies with experimental spectra, mainly due to the fact that most spectral values correspond to energy differences which are usually more accurate due to cancellations of errors. Recently, calculations beyond the CCSD(T) level improved agreement with experiment for the spectra of H_2–CO by nearly an order of magnitude[69] and similar improvements are probably possible for the water dimer.

Summarizing, we may conclude that, as reported previously,[18] the CCpol-8s potential still constitutes the best available rigid-monomer potential for the description of the VRT levels of both $(H_2O)_2$ and $(D_2O)_2$. The VRT levels from the flexible-monomer CCpol-8s*f* potential are, on average, equally good. Also the frequency shifts of the monomer vibrations calculated with the CCpol-8s*f* potential agree well with the experimental data extracted from IR spectra (with some uncertainties, as indicated).

ACKNOWLEDGMENTS

Dr. F. Gatti is acknowledged for helpful discussions. K. Sz. was partly supported by the National Science Foundation (NSF) Grant No. CHE-0848589.

[1] K. Szalewicz, C. Leforestier, and A. van der Avoird, Chem. Phys. Lett. **482**, 1 (2009).
[2] H. A. Gebbie, W. J. Burroughs, J. Chamberlain, J. E. Harries, and R. G. Jones, Nature (London) **221**, 143 (1969).
[3] Y. Scribano, N. Goldman, R. J. Saykally, and C. Leforestier, J. Phys. Chem. A **110**, 5411 (2006).
[4] U. Gora, R. Podeszwa, W. Cencek, and K. Szalewicz, J. Chem. Phys. **135**, 224102 (2011).
[5] Z. S. Huang and R. E. Miller, J. Chem. Phys. **91**, 6613 (1989).
[6] L. B. Braly, K. Liu, M. G. Brown, F. N. Keutsch, R. S. Fellers, and R. J. Saykally, J. Chem. Phys. **112**, 10314 (2000).
[7] N. Goldman, R. S. Fellers, M. G. Brown, L. B. Braly, C. J. Keoshian, C. Leforestier, and R. J. Saykally, J. Chem. Phys. **116**, 10148 (2002).
[8] F. N. Keutsch, N. Goldman, H. A. Harker, C. Leforestier, and R. J. Saykally, Mol. Phys. **101**, 3477 (2003).
[9] K. Kuyanov-Prozument, M. Y. Choi, and A. F. Vilesov, J. Chem. Phys. **132**, 014304 (2010).
[10] H. Chen, S. Liu, and J. C. Light, J. Chem. Phys. **110**, 168 (1999).
[11] R. S. Fellers, C. Leforestier, L. B. Braly, M. G. Brown, and R. J. Saykally, Science **284**, 945 (1999).
[12] R. S. Fellers, C. Leforestier, L. B. Braly, M. G. Brown, and R. J. Saykally, J. Chem. Phys. **110**, 6306 (1999).
[13] G. C. Groenenboom, E. M. Mas, R. Bukowski, K. Szalewicz, P. E. S. Wormer, and A. van der Avoird, Phys. Rev. Lett. **84**, 4072 (2000).
[14] E. M. Mas and K. Szalewicz, J. Chem. Phys. **104**, 7606 (1996).
[15] M. Jeziorska, P. Jankowski, K. Szalewicz, and B. Jeziorski, J. Chem. Phys. **113**, 2957 (2000).

[16]E. M. Mas, R. Bukowski, K. Szalewicz, G. C. Groenenboom, P. E. S. Wormer, and A. van der Avoird, J. Chem. Phys. **113**, 6687 (2000).
[17]G. C. Groenenboom, P. E. S. Wormer, A. van der Avoird, E. M. Mas, R. Bukowski, and K. Szalewicz, J. Chem. Phys. **113**, 6702 (2000).
[18]W. Cencek, K. Szalewicz, C. Leforestier, R. van Harrevelt, and A. van der Avoird, Phys. Chem. Chem. Phys. **10**, 4716 (2008).
[19]X. Huang, B. J. Braams, J. M. Bowman, R. E. A. Kelly, J. Tennyson, G. C. Groenenboom, and A. van der Avoird, J. Chem. Phys. **128**, 034312 (2008).
[20]Z. S. Huang and R. E. Miller, J. Chem. Phys. **88**, 8008 (1988).
[21]B. Nelander, J. Chem. Phys. **88**, 5254 (1988).
[22]C. Leforestier, F. Gatti, R. S. Fellers, and R. J. Saykally, J. Chem. Phys. **117**, 8710 (2002).
[23]G. Murdachaew and K. Szalewicz, Faraday Discuss. **118**, 121 (2001).
[24]G. Murdachaew, R. Bukowski, and K. Szalewicz, Phys. Rev. Lett. **88**, 123202 (2002).
[25]K. Szalewicz, G. Murdachaew, R. Bukowski, O. Akin-Ojo, and C. Leforestier, in *Lecture Series on Computer and Computational Science: ICCMSE 2006*, edited by G. Maroulis, and T. Simos (Brill Academic, Leiden, 2006), Vol. 6, pp. 482–491.
[26]X. Huang, B. J. Braams, and J. M. Bowman, J. Phys. Chem. A **110**, 445 (2006).
[27]B. Jeziorski, R. Moszyński, and K. Szalewicz, Chem. Rev. **94**, 1887 (1994).
[28]K. Szalewicz, K. Patkowski, and B. Jeziorski, Struct. Bonding (Berlin) **116**, 43 (2005).
[29]S. S. Xantheas and T. Dunning, J. Chem. Phys. **99**, 8774 (1993).
[30]G. S. Tschumper, M. L. Leininger, B. C. Hoffman, E. F. Valeev, H. F. Schaefer III, and M. Quack, J. Chem. Phys. **116**, 690 (2002).
[31]R. Bukowski, K. Szalewicz, G. C. Groenenboom, and A. van der Avoird, Science **315**, 1249 (2007).
[32]R. Bukowski, K. Szalewicz, G. C. Groenenboom, and A. van der Avoird, J. Chem. Phys. **128**, 094313 (2008).
[33]R. Bukowski, K. Szalewicz, G. C. Groenenboom, and A. van der Avoird, J. Chem. Phys. **128**, 094314 (2008).
[34]C. Leforestier, R. van Harrevelt, and A. van der Avoird, J. Phys. Chem. A **113**, 12285 (2009).
[35]K. T. Tang and J. P. Toennies, J. Chem. Phys. **80**, 3726 (1984).
[36]O. L. Polyansky, P. Jensen, and J. Tennyson, J. Chem. Phys. **105**, 6490 (1996).
[37]F. Gatti and C. Iung, Phys. Rep. **484**, 1 (2009).
[38]W. Klopper, M. Quack, and M. A. Suhm, Chem. Phys. Lett. **261**, 35 (1996).
[39]W. Klopper, M. Quack, and M. A. Suhm, J. Chem. Phys. **108**, 10096 (1998).
[40]F. T. Smith, Phys. Rev. Lett. **45**, 1157 (1980).
[41]Z. Bačić, D. Watt, and J. C. Light, J. Chem. Phys. **89**, 947 (1988).
[42]H. Wei and T. Carrington, J. Chem. Phys. **107**, 2813 (1997).
[43]H. Wei and T. Carrington, Chem. Phys. Lett. **287**, 289 (1998).
[44]W. H. Press, B. P. Flannery, S. A. Teukolsky, and W. T. Vetterling, *Numerical Recipes* (Cambridge University Press, Cambridge, 1986).
[45]Z. Bačić and J. C. Light, J. Chem. Phys. **85**, 4594 (1986).
[46]Z. Bačić and J. C. Light, J. Chem. Phys. **87**, 4008 (1987).
[47]G. T. Fraser, J. Chem. Phys. **90**, 2097 (1989).
[48]G. Brocks, A. van der Avoird, B. T. Sutcliffe, and J. Tennyson, Mol. Phys. **50**, 1025 (1983).
[49]C. Leforestier, L. B. Braly, K. Liu, M. J. Elrod, and R. J. Saykally, J. Chem. Phys. **106**, 8527 (1997).
[50]T. R. Dyke, J. Chem. Phys. **66**, 492 (1977).
[51]C. Lanczos, J. Res. Natl. Bur. Stand. **45**, 255 (1950).
[52]D. O. Harris, G. G. Engerholm, and W. D. Gwinn, J. Chem. Phys. **43**, 1515 (1965).
[53]L. B. Braly, J. D. Cruzan, K. Liu, R. S. Fellers, and R. J. Saykally, J. Chem. Phys. **112**, 10293 (2000).
[54]F. N. Keutsch, L. B. Braly, M. G. Brown, H. A. Harker, P. B. Petersen, C. Leforestier, and R. J. Saykally, J. Chem. Phys. **119**, 8927 (2003).
[55]B. E. Rocher-Casterline, L. C. Ch'ng, A. K. Mollnera, and H. Reisler, J. Chem. Phys. **134**, 211101 (2011).
[56]E. Zwart, J. J. ter Meulen, and W. L. Meerts, Chem. Phys. Lett. **166**, 500 (1990).
[57]E. N. Karyakin, G. T. Fraser, and R. D. Suenram, Mol. Phys. **78**, 1179 (1993).
[58]J. B. Paul, R. A. Provencal, and R. J. Saykally, J. Phys. Chem. A **102**, 3279 (1998).
[59]M. J. Smit, G. C. Groenenboom, P. E. S. Wormer, A. van der Avoird, R. Bukowski, and K. Szalewicz, J. Phys. Chem. A **105**, 6212 (2001).
[60]J. B. Paul, R. A. Provencal, C. Chapo, K. Roth, R. Casaes, and R. J. Saykally, J. Phys. Chem. A **103**, 2972 (1999).
[61]F. Huisken, M. Kaloudis, and A. Kulcke, J. Chem. Phys. **104**, 17 (1996).
[62]U. Buck and F. Huisken, Chem. Rev. **100**, 3863 (2000).
[63]J. Ceponkus, P. Uvdal, and B. Nelander, J. Phys. Chem. A **112**, 3921 (2008).
[64]C. Leforestier, Phil. Trans. R. Soc. London, Ser. A **370**, 2675 (2012).
[65]G. Murdachaew, R. Bukowski, P. Jankowski, O. Akin-Ojo, C. Leforestier, and K. Szalewicz, "Water pair potential with flexible monomers from symmetry-adapted perturbation theory" (to be published).
[66]A. Shank, Y. Wang, A. Kaledin, B. J. Braams, and J. M. Bowman, J. Chem. Phys. **130**, 144314 (2009).
[67]Y. Wang and J. M. Bowman, Chem. Phys. Lett. **419**, 1 (2010).
[68]R. Podeszwa, K. Patkowski, and K. Szalewicz, Phys. Chem. Chem. Phys. **12**, 5974 (2010).
[69]P. Jankowski, A. R. W. McKellar, and K. Szalewicz, Science **336**, 1147 (2012).
[70]E. Zwart, J. J. ter Meulen, W. L. Meerts, and L. H. Coudert, J. Mol. Spectrosc. **147**, 27 (1991).
[71]G. T. Fraser, Int. Rev. Phys. Chem. **10**, 189 (1991).